NTNU
Norwegian University of
Science and Technology

Modelling of Aerodynamic Drag in Alpine Skiing

Ola Elfmark

Master of Science
Submission date: June 2017
Supervisor: Jon Andreas Støvneng, IFY
Co-supervisor: Lars Roar Sætran, EPT

Norwegian University of Science and Technology
Department of Physics

Abstract

Most of the breaking force in the speed disciplines in alpine skiing is caused by the aerodynamic drag, and a better knowledge of the drag force is therefore desirable to gain time in races. In this study a complete database of how the drag area (C_DA) changes, with respect to the different body segments, was made and used to explain a complete body motion in alpine skiing. Three experiments were performed in the wind tunnel at NTNU, Trondheim. The database from a full body measurement on an alpine skier from the Norwegian Ski Federation (NSF), was used to make a numerical model, with the angles in the different body segments as input, to compute the C_DA. The model was validated with an uncertainty of ±3%. A new method for calculating the frontal area of an alpine skier inside a wind tunnel was introduced with an uncertainty of $\pm 0.012 m^2$.

One of the most interesting results presented in this thesis is that the C_DA values were increasing when the arm angle approaches zero. This affects some of the flight positions used in competitive alpine skiing, where the athletes are instructed to jump with the arms straight down on the side of the body. Different flight positions were evaluated and possible new flight positions were suggested. The aerodynamic drag in a turning position was discussed briefly with the tendency that the the change in C_DA is proportional to the change in the frontal area through the turn. However, ground effects were not taken into account.

The last experiment had four different test subjects from NSF and showed that the percentage change in C_DA from the highest to the lowest position was constant and that the drag coefficient (C_D) was constant, for the different test subjects. The only parameter one then needs to vary for personal adjustments of the numerical model is the frontal area of the test subjects in the most upright position. By only changing the frontal area as a parameter for the four different test subjects in the numerical model, it still had an uncertainty of ±3%. The results from the wind tunnel and the numerical model were compared to data from a preliminary field experiment, a flight sequence for one of the test subjects. The results from the experiments in the wind tunnel and the numerical model were in accordance with results from the field experiment.

Sammendrag

Den største delen av de bremsende kreftene som virker på en alpinist i fartsdisiplinene i alpint er luftmotstand. Bedre kunnskap om luftmotstand er med det ønskelig for å kunne vinne tid i renn. I denne studien har det blitt lagd en database på hvordan dragarealet (C_DA) endrer seg for de ulike kroppsdelene brukt til å beskrive en fullstendig kroppsbevegelse i alpint. Tre eksperimenter har blitt gjennomført i vindtunnelen ved Norges teknisk-naturvitenskapelige universitet (NTNU). Et preliminært eksperiment samt et eksperiment der en full kroppsbevegelse ble målt på en aplinutøver fra Norges Skiforbundet (NSF) lagde databasen for hvordan C_DA-verdiene endret seg for de ulike kroppsdelene. Disse resultatene utgjorde databasen til den numeriske modellen som brukte vinkler i de ulike kroppssegmentene som input. Den numeriske modellen ble validert med en usikkerhet på ±3%. En ny metode for måling av frontalareal av en utøver i vindtunnel ble introdusert med en usikkerhet på $\pm 0.012 m^2$.

Et av de mest interessante resultatene var at C_DA-verdiene øker når armvinkelen går mot null. Dette vil påvirke enkelte posisjoner brukt i svev der alpinistene er instruert til å holde armene tett inntil kroppen. Forskjellige svevposisjoner ble testet og evaluert og nye mulige svevposisjoner ble foreslått. Luftmotstanden i en svingbevegelse ble sett på og tendensen var at C_DA i en sving endres proporsjonalt med endringen i frontalareal. Effekter som vil påvirke da alpinisten er nære bakken ble ikke tatt hensyn til her.

Det siste eksperimentet hadde fire alpinister fra NSF og viste at den prosentvise endringen i C_DA fra den høyeste til den laveste posisjonen var den samme for alle utøverne og at drag coefficienten (C_D) var den samme for alle utøverne i de ulike posisjonene testet. Dette gjorde at den eneste parameteren som måtte endres i den numeriske modellen fra utøver til utøver var frontalarealet i den høyeste posisjonen. Ved å kun endre denne parameteren på de fire utøverne hadde den numeriske modellen en usikkerhet på ±3%. Resultatene fra vindtunnelen og den numeriske modellen ble sammenlignet med feltresultater fra et svev for en av utøverne. Resultatene viste en klar sammenheng mellom verdier målt i vindtunnellen, estimert av modellen og målt ute i felt.

Preface

This is a master thesis on modelling of aerodynamic drag in alpine skiing at NTNU as a part of a 5 year study program study program MLREAL, carried out during the spring semester of 2017. This project has been carried out for the Norwegian ski federation under the supervision of Robert Reid. The idea for this thesis was brought up after mail correspondence in January 2016. I would like to thank him for this opportunity and their help, guidance and inspiration through this project.

Trondheim, 2017-06-15

Ola Elfmark

Acknowledgements

First of all I want to thank Lars Morten Bardal for great help and supervision during this the master thesis, both with theoretical and practical work. I also want to thank Lars Roar Sætran for weekly meetings and Jon Andreas Støvneng for approval of this project from the department of physics.

I would like to thank Sindre Kristian Alvsvåg, Simon Alexander Milne, Rolf Klokkerengen, Gisle Roel Bye, Jørgen Sunnvoll and Ferdinand Tomek Marnburg for participating in a preliminary wind tunnel experiment, Mattis Håklev for a full day testing of arms and elbows, Mina Fuerst Holtmann from the Norwegian World Cup team for two long days of testing and the guys from the Norwegian European Cup team, Stian Saugestad, Marcus Fossland, Tomas Markegård and Henrik Røa for a whole day of testing.

Finally, but not less important I want to thank my family for great support through five years at NTNU and my good friend Øyvind Paulsen for the support, knowledge sharing, collaboration and great fun through the last five years.

Contents

Chapter 1

Introduction

Alpine skiing is a highly competitive sport, only a hundredth of a second can be the difference between first and second place. Good tools to analyze the performance are therefore important to get an understanding of where an athlete is gaining and losing time. The Norwegian ski federation (NSF) uses a differential global navigation satellite system (dGNSS), later on described, to analyze the performance and calculate the trajectory of the skier. By calculating the derivative of the velocity vector, the system can also estimate the total instant breaking force acting on the skier. The breaking force is the sum of the aerodynamic drag force and the ski-snow friction force. The technology can however not determine how much of the breaking force is due to the ski-snow friction and how much that is due to the aerodynamic drag force. The drag force can be as large as 80% of the total breaking force in the speed disciplines downhill and super G, and a better understanding of the drag force is then desirable.

Figure 1.1: Alpine skier in a downhill competition. Foto: GEPA Pictures

Although it is known that the aerodynamic drag causes most of the breaking force in the speed disciplines, most of the research done in alpine skiing is done on ski-snow friction. Determination of the drag force is complex. It is determined by variables such as the relative velocity, the frontal area of the skier, the shape of the skier and the skier's suit and equipment. Many of these factors are continuously changing throughout a race. The factors frontal area, shape of the skier, the skier's suit and equipment are all compiled in the variable called the drag area (C_DA). Investigation of different ways to model the drag force on an alpine skier is previously carried out by M. Supej et al. [1] and F. Meyer et al. [2]. With the help of a model of the drag area one should be able to determine both the drag force and then also the ski-snow friction force and thereby determine what is causing the time loss.

A good understanding of how the drag is changing with respect to the different segments of a human body is also desirable in a race situation for a alpine skier. A skier with good knowledge of how the drag depends on the body position will have an advantage compared to others by always choosing the most aerodynamic position possible. The coaches could also use this knowledge when analyzing videos after a race.

The aim of this thesis is to make a complete data base of how the drag area is changing with respect to the different body segments, used to explain a complete body motion in alpine skiing. Then use this data base to make a programmatic model that uses the angles between the different body segments as input to compute C_DA. The theoretical background for this thesis are presented in the first part. Experimental setup, method and results are then presented before the numerical model is presented and validated. In the last part a preliminary experiment in the field, with the dGNSS, is compared to results from the wind tunnel and the numerical model.

Chapter 2

Theory

This chapter gives the reader an overview of the theoretical background for this thesis. The chapter has four main parts, first is an introduction to forces acting on an alpine skier, second comes an overview of the motion tracking system used by NSF, thirdly, the theory of flow around cylindrical shapes and lastly an overview of the theory of blockage correction in a wind tunnel.

2.1 Forces in Alpine Skiing

Looking at the forces working on an alpine skier, one has to start by considering Newtons second and third law. From this, the equation of motion for an alpine skier can be formulated as

$$\Sigma \vec{F} = \vec{F}_a + \vec{F}_r = m\vec{a}, \tag{2.1}$$

where $\vec{F}_a$ represents the applied forces and $\vec{F}_r$ the reaction forces. $\vec{F}_r$ follows directly from Newtons third law [3]. The applied forces $\vec{F}_a$ can be written as

$$\vec{F}_a = \vec{F}_G + \vec{F}_f + \vec{F}_D + \vec{F}_c, \tag{2.2}$$

where $\vec{F}_G$ is the gravitational force, $\vec{F}_D$ is the aerodynamic drag, $\vec{F}_f$ is the ski-snow friction and $\vec{F}_c$ the centripetal force. Combining with equation (2.1) and (2.2) we get

$$\Sigma \vec{F} = m\vec{a} = \vec{F}_G + \vec{F}_f + \vec{F}_D + \vec{F}_c + \vec{F}_r. \tag{2.3}$$

The forces are shown in Figure 2.1. The gravitational force is the greatest contribution for the skiers motion down a hill and can be written as

$$\vec{F}_G = m\vec{g}, \tag{2.4}$$

with m as the skiers mass and gravitational acceleration $\vec{g} \simeq 9.81 m/s^2$. When the skier has contact with the snow

$$\vec{F}_r = \vec{F}_{G_y} = \vec{F}_G cos\alpha. \tag{2.5}$$

The turns are essential elements in alpine skiing. A curved motion like a turn requires a force with direction pointing toward the center of the turn and this is represented with an accelerated motion. This force is the centripetal force and it is defined as

$$\vec{F}_c = m\frac{V_{rel}^2}{r}, \tag{2.6}$$

where m is the mass of the skier, V_{rel} the relative velocity and r is the radius of the turn. The centripetal acceleration is defined as $a_c = V_{rel}^2/r$.

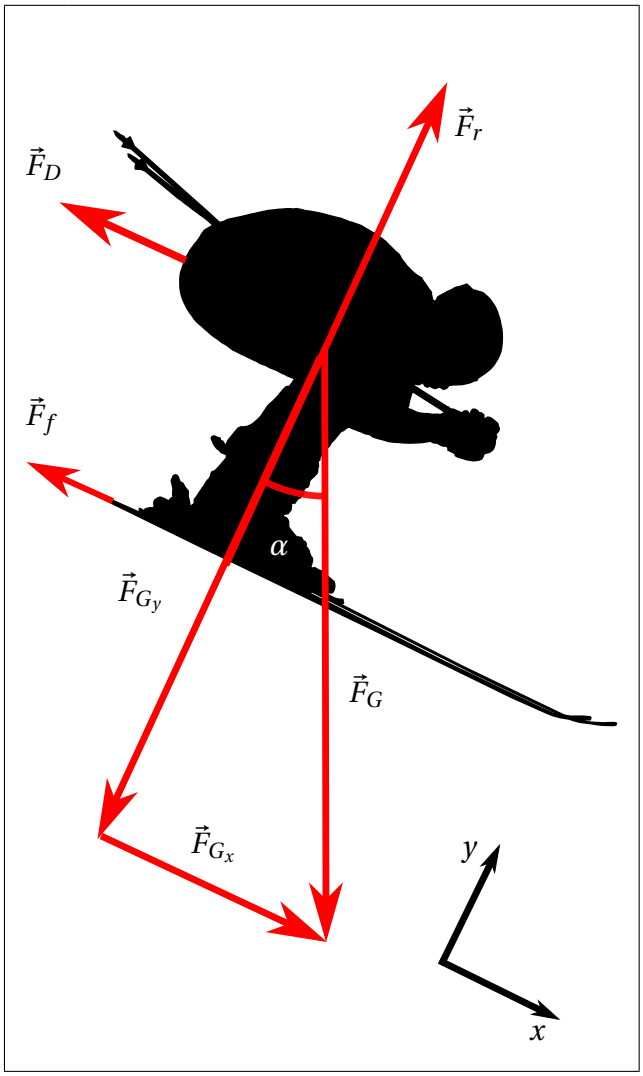

Figure 2.1: Gravitational force, reaction force, aerodynamic drag and ski-snow friction acting on an alpine skier.

2.1.1 Aerodynamic Drag

An object that is passing through a viscous fluid will experience a resistive force that counteract the motion. This is the drag force $\vec{F}_D$. The drag force has two main components, the friction drag force $\vec{F}_{fd}$ and the pressure drag force $\vec{F}_{pd}$. The friction drag is due to the viscous friction between the air and the surface of the skier and it is determined by the friction forces in the boundary layer [3]. The surface properties, the Reynolds number and the surface area of the material determine the friction drag.

When a bluff body is moving in a fluid at high Reynolds numbers the pressure in front of the object will be greater than the pressure behind the object due to separation. Combining the friction drag force and the pressure drag force the total drag force can be formulated as

$$\vec{F}_D = \frac{1}{2}\rho V_{rel}^2 C_D A, \tag{2.7}$$

where ρ is the density, V_{rel} is the relative velocity, C_D is the drag coefficient and A_p is the projected frontal area of the skier [3]. The Reynolds number is defined as

$$Re = \frac{VL}{\nu},$$

where V is the characteristic velocity, L is the characteristic length and ν is the kinematic viscosity. The goal for an alpine skier will be to have as low $\vec{F}_D$ as possible. From a mathematical point of view, $\vec{F}_D$ from equation (2.7) is easily reduced by letting $V_{rel} \to 0$, but this will not be an option for an alpine skier. Since the density ρ will be determined by the ambient pressure and temperature, the two remaining variables one can manipulate are the frontal area A and the drag coefficient C_D. The drag coefficient is dependent on the Reynolds number, surface roughness and the shape of the skier. Combining these two variables one gets $\mathrm{C_DA}$.

Studies show that typical C_DA values for an alpine skier range from $C_DA = 0.15 \pm 0.02\ m^2$ near the most aerodynamic position to $C_DA = 0.35 \pm 0.06\ m^2$ in an upright position [4]. For accurate measurements of the total drag force in the field, computation of the relative velocity is important since $\vec{F}_D \propto V_{rel}^2$. A skier is turning through the whole race and the relative velocity is changing due to the difference in the wind velocity. For accurate measurements of the relative velocity some kind of sensors for measurement of the wind velocity must be implemented. If there is no wind the relative velocity can be estimated fairly well as the total velocity.

2.1.2 Ski-Snow Friction

The snow friction force can be separated into two regimes [3], dry friction and wet friction. Dry friction is the frictional interaction at the ski-snow interface and wet friction is when the contact surface is covered by a lubricating water film. For friction between a solid and its supporting surface, the friction force can be modeled as the Coulomb friction

$$\vec{F}_f = \mu \vec{F}_r, \tag{2.8}$$

where μ is the coefficient of kinetic friction and $\vec{F}_r$ is the reaction force. It is important to separate the kinetic friction from the static friction. Kinetic friction is applicable when the object is moving and static friction when the object is resting. The maximal static friction is usually larger than kinetic friction. Heat is generated due to the kinetic friction between the ski and the snow. If the ski-snow contact surface is not completely covered by a lubricating water film, mixed friction occurs. Due to the frictional heating there may exist dry friction at the front of the ski and wet friction towards the rear of the ski. This makes the friction coefficient vary along the length of the ski. The mean friction coefficient can then be expressed as

$$\mu_1 = \frac{1}{\vec{F}_r} \sum_{i=1}^{n} \vec{F}_{f,i}. \tag{2.9}$$

Combining equation (2.8) and (2.9), the friction force can be modeled as

$$\vec{F}_f = \mu_1 \vec{F}_r. \tag{2.10}$$

When using this model the friction force ($\vec{F}_{f,i}$ i=1,...n) for separate segments of the ski must be estimated. The kinetic friction coefficient μ_1 is dependant on the speed. The kinetic friction coefficient on snow has previously been measured both in field studies using skis gliding on snow and in the laboratory using a rotational friction instrument consisting of a rotational disk and a snow pan by D.A Moldestad [5]. The results show that $0.02 \leq \mu \leq 0.11$ and that for dry, cold snow μ almost remains constant for speeds up to 10m/s while μ changes rapidly already for low speeds under wet conditions [5]. This is because under wet snow conditions wet friction is taking place at an earlier stage than under dry conditions. W. Nachbauer et al. [6] present an overview over friction measurements in the field. Some of the results are shown in Table 2.1.

Table 2.1: Overview of the friction coefficient (μ) during straight running (a) and turning (b), by W. Nachbauer et al. [6].

(a)

Velocity $[m/s]$	μ
8.0-22	0.02-0.10
0.5-10	0.02 (dry snow)
0.5-10	0.03-0.10 (wet snow)

(b)

Turning type	μ
Carving	0.20-0.30
Downhill racing turn	0.45

2.1.3 Summary

By combining equation (2.3)-(2.7) and (2.10) one can model the total force on an alpine skier as

$$\Sigma\vec{F} = m\vec{g} + \mu_1 m\vec{g}cos\alpha + \frac{1}{2}\rho V_{rel}^2 AC_D + m\frac{V_{rel}^2}{r} + m\vec{g}cos\alpha,$$

which can be simplified to

$$\Sigma\vec{F} = ((\mu_1 + 1)cos\alpha + 1)m\vec{g} + (\frac{1}{2}\rho AC_D + \frac{m}{r})V_{rel}^2. \tag{2.11}$$

2.2 Motion Tracking System

A skier's momentum is continuously changing when moving down a hill with high velocity. A good understanding of a skier's momentum (the velocity and direction along the trajectory), the center of mass (CoM) and the external forces acting on the skier (ground reaction, gravity, friction and drag forces) can improve a race in alpine skiing [7]. Sensors for measurement of trajectory and CoM is already well established and used by many alpine skiing teams. The biggest disadvantage with this system is that it is fairly large and interacting with the skier and the performance, so it cannot be used in competitions.

Figure 2.2: dGNSS on the back of an alpine skier. Foto: NSF.

The dGNSS used by NSF is shown in Figure 2.2. To obtain reliable data with high accuracy of the skier's trajectory and CoM a combination of dGNSS and inertial sensors have been used by M. Gilgien et al. [7].

dGNSS is a collective term for a differential global navigation satellite system. Studies by M. Gilgien et al. [7, 8] make use of the well known American global navigation satellite system (GPS) and the Russian global navigation satellite system (GLONASS). To get better accuracy it is desirable to use antennas and receivers which can receive signals from more than one satellite system. In order to get accurate data at least four satellites are needed. The American GPS consists of 32 satellites and GLONASS of 24, but not all of them are in view at the same time all over the world. When using this method at least two units are required. One unit is mounted on the athlete and the other units are stationed as close as possible to the course.

The dGNSS is capturing the skier's trajectory, assuming that the skier is a point mass [8]. To get an accurate trajectory it is desirable to place the antenna at the CoM, but this is not possible because the CoM position is changing with time. In studies by M. Gilgien et al. [7–9] the antenna is proposed to either be placed at the skiers back or at the head. Placing the antenna on the skier's head, as shown in Figure 2.3, minimizes the shading and gives maximal use of the available satellites. This position gives the most accurate antenna position [9].

Figure 2.3: Skier with the antenna for the dGNSS mounted on the head. Foto: NSF.

One model for the CoM with the antenna on the head is based on the approximation of the bio mechanical phenomenon of skier's incline laterally in order to balance the radial force during a turn [7]. The skier's inclination is then modelled by an inverted pendulum shown in Figure 2.4. When turning, the pendulum is deflected from a neutral position because of the lateral inclination of the skier. Studies from M. Gilgien [8] show that the CoM position vector of the dGNSS corresponds to 53% of $\vec{L}$.

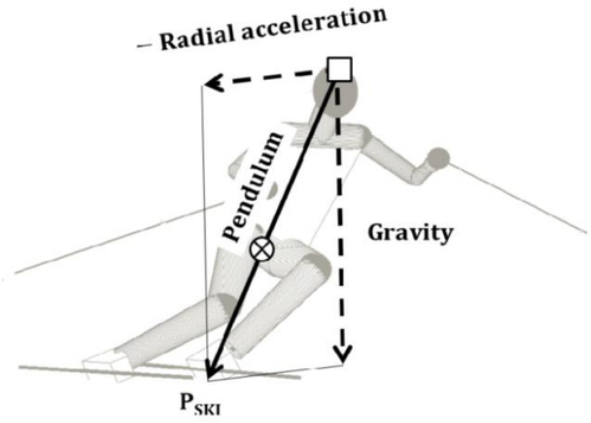

Figure 2.4: The pendulum model approximating of the CoM. □ being the antenna and ⊗ the CoM, from M. Gilgien et al. [7].

2.3 Flow Around Cylindrical Shapes

The body of an alpine skier can roughly be modeled as a combination of cylinders with different lengths and diameters. The fluid flow around two cylinders in close proximity is complex. A review of studies of flow around cylinders placed close to each other is made by D. Sumner [10].

Related to alpine skiing the aerodynamic interaction between body parts can either be modeled as a case where two cylinders are side-by-side, for example when modelling two legs, or as a staggered pair of cylinders, for example arms interacting with the upper body. The geometry in these two cases are shown in Figure 2.5.

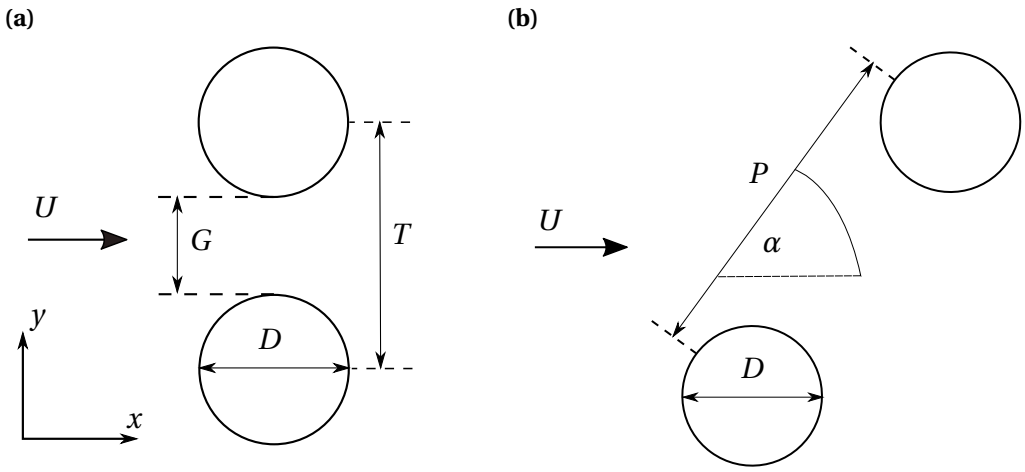

Figure 2.5: Defined geometric of two cylinders of equal diameter. Figure (a) is the side-by-side configuration and Figure (b) the staggered configuration.

2.3.1 Side-by-Side Configuration

In the side-by-side configuration the fluid behaviour has been modelled as a function of the ratio T/D. As shown in Figure 2.5, T is the center-to-center length of the cylinders and D is the diameter of the cylinders. There are three different main flow patterns based on this ratio. The different flow patterns and their ratio are shown in Table 2.2.

Table 2.2: Different flow patterns and their ratio for the side-by-side configurations of two cylinders.

Flow pattern	Range
Single-bluff-body behaviour	1≤ T/D < 1.1-1.2
Biased flow pattern	1.1-1.2 < T/D < 2.0-2.2
Parallel vortex streets	T/D > 2.0-2.2

For a single-bluff-body behaviour the two cylinders have a behaviour similar to a single bluff-body. For the case $T/D = 1$ the cylinders are touching and the behaviour is slightly different from the rest of the range. The Biased flow pattern is characterized by an asymmetrical flow biased towards one of the cylinders. The deflection of the biased gap flow varies with T/D. For the parallel vortex sheets the cylinders behave as if they are independent of each other.

The data of the mean drag coefficient represented by D. Sumner [10] show that for the Single-bluff-body behaviour the drag coefficient is high for $T/D = 1$ (touching cylinders) and decreasing. For the biased flow pattern the drag coefficient for both cylinders are increasing to a higher value than for a single cylinder. In the range of the parallel vortex streets the mean drag coefficient for both cylinders approaches the value of a single cylinder.

2.3.2 Staggered Configuration

As shown in Figure 2.5, P is the center-to-center length of the cylinders, D is the diameter of the cylinders and α is the angle of incidence. In the Staggered confirmation the fluid behaviour is modelled as a function of α for different ratios P/D. The angle α range from 0°, a tandem configuration, to 90° being the side-by-side configuration. The data presented by D. Sumner [10] show that there is a big difference in the mean drag coefficient between the two cylinders for incidence angles $\alpha < 30°$ and a small difference for $\alpha > 30°$ for $P/D < 1.5$.

2.4 Blockage Correction

Doing experiments on an alpine skier in a closed wind tunnel, the test subject will take up some of the space in the cross section of the wind tunnel. The flow around the subject in a wind tunnel will act differently than outside in an alpine hill because of the walls in the wind tunnel. This error is called blockage error and it has to be taken into account when doing measurements in a wind tunnel [11]. The types of effect that make a flow in a wind tunnel different from a free stream flow are complex. The three types that affect the flow the most are Solid blockage, wake blockage and tunnel wall boundary-layer blockage.

In **solid blockage**, the subject will make the effective cross section smaller and by that accelerate the flow, due to continuity and Bernoulli's equation. The increase in the free stream velocity will increase the drag force.

The **wake blockage** is due to the loss of momentum in the wake. To satisfy the continuity equation the velocity in the flow around the test subject must have an increase, because the velocity within the wake is lower than for a free stream flow. The increase in the velocity in the flow yields a greater drag force.

For **tunnel wall boundary-layer blockage**, an increase of velocity is caused by the growth of the boundary layers, this causes a drop in static pressure. The resulting pressure gradient causes a force in the same direction as the drag force and increases by that the drag force.

Chapter 3

Experimental Setup and Methods

3.1 Wind Tunnel Measurements

The experiments were carried out in a wind tunnel at the Norwegian University of Science and Technology (NTNU) in Trondheim. The test section of the wind tunnel is 1.8 m high, 2.7 m wide and 12.5 m long and uses a 220-kW centrifugal fan to produce wind speed up to 25 m/s. The drag force $\vec{F}_D$ was measured with a Schenck six-component force balance and the wind speed with a pitot-probe mounted upstream in the wind tunnel. Alpine bindings were mounted directly to the force platform. A live video feed showing the side and rear view of the skier was projected on the wind tunnel floor in front of the skier. Guidelines were added in order to help the test subject keep a consistent position. A white plate was mounted on the side wall of the tunnel so it would be easier for the test subject to see the guidelines.

The velocity was set to be approximately 20 m/s and the sampling time to be 30 s, so the test subject should be able to maintain the same position throughout the sample time. For every position, three measurements were performed and the mean value was used. At the start and the end of each sample a picture was taken of the test subject. This was done to evaluate if the test subject had maintained the desired position and to estimate the frontal area. The angles of the knees, hips, arms and elbow were measured manually in every picture. The pictures were taken as shown in Figure 3.1. In order to make a model for the drag force on an alpine skier based on body position, the body of the skier has to be divided into the different body segments which are explained in appendix A.

A reference position was chosen for all experiment, the reference position is shown in Figure 3.1.

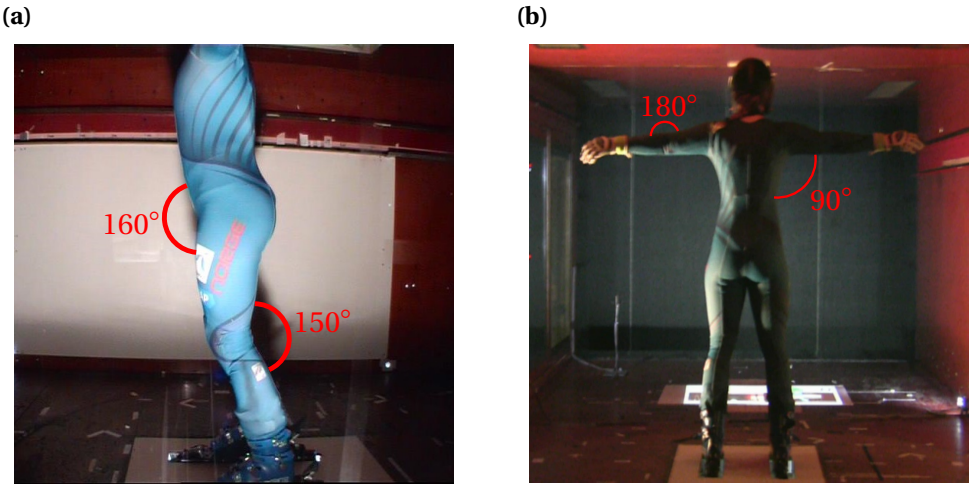

Figure 3.1: Test subject standing in the reference position. Picture (a) showing the side picture and picture (b) the rear picture.

The angles of the hip and the knee were considered dependent on each other and the measurement of the knee flexion and the hip flexion were taken together. With a few assumptions, a realistic range of movement of the hips and knees was defined as shown in Figure 3.2.

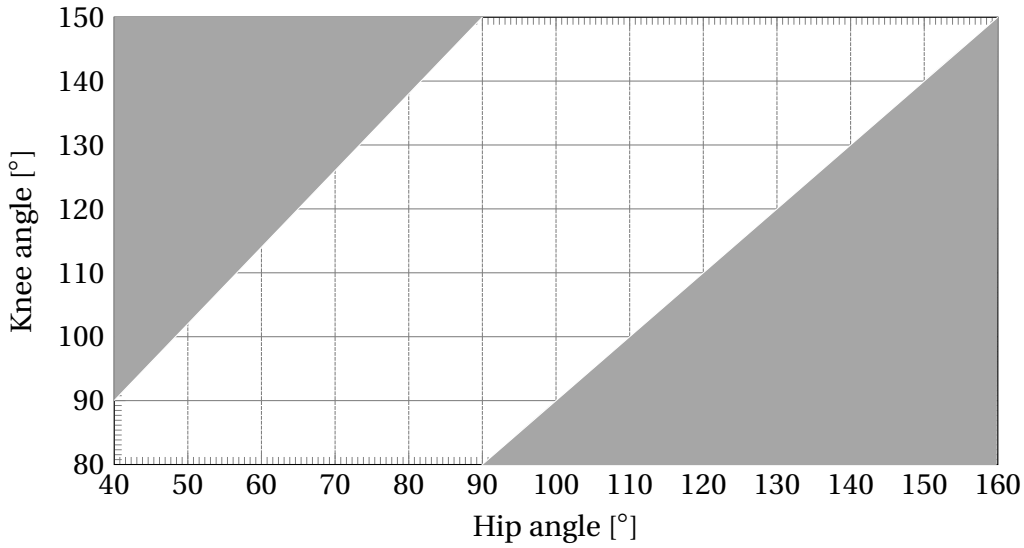

Figure 3.2: Range of movement of the hip-knee motion in alpine skiing.

The first assumption was that a skier never has a hip angle below 90° if his knee angle is as large as possible (here 150°). The second assumption was that for holding the balance and control of the CoM the hip angle has to be no more than 10° larger than the knee angle.

Then the lowest position was measured. The lowest and most aerodynamic position in alpine skiing is defined as the hockey position and shown in Figure 3.3. The knee angle and the hip angle were defined as 180° in an upright position and range down to 0° by flexion. The arm angle was defined as 90° with the arms straight out to the side and 0° with the arms along the torso. The shoulder and elbow were both defined as 180° when pointing to the side and 90° when pointing forward by shoulder protraction and elbow flexion. The anatomical definitions of movements are described in appendix A. A reference position was chosen to an upright position with both arms to the sides. This corresponded to 150° in knee angle, 160° in hip angle, 90° in arm angle and 180° in elbow angle.

Figure 3.3: An alpine skier in a good hockey position. Foto: GEPA Pictures.

In the authors thesis work [12] the movement of the shoulder was assumed to be independent of the other body segments. After consulting with one of the downhill coaches of NSF this assumption was neglected. The movement of the shoulder in alpine skiing is used to adjust the upper arm (from shoulder to the elbow) to point straight down to keep the balance, shown in Figure 3.4. So the movement of the shoulder can be explained from the hip angle and the arm angle and is therefore neglected in this model. The angles in the ankles were assumed constant in the model.

(a) **(b)** **(c)**

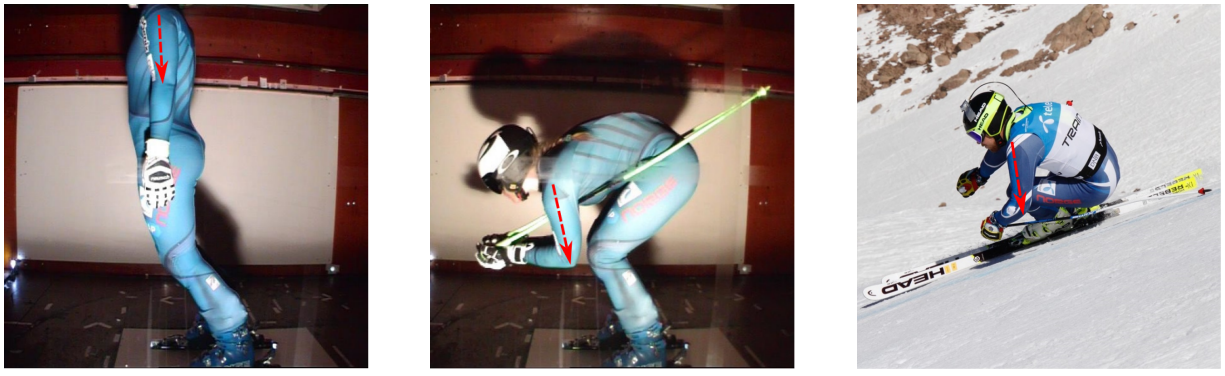

Figure 3.4: Shoulder adjustments in different positions to keep the upper arm pointing down. Picture (a) and (b) taken from experiments. Picture (c) is owned by NSF.

3.2 Frontal Area Measurements

Pictures from a camera behind the test subject, picture (b) in Figure 3.1, was used for the frontal area measurements. A setup with small lamps was used to illuminate the background, and create a sharp silhouette. The resulting image is shown in Figure 3.5. The frontal area was calculated by counting black pixels from a binary image. A calibration factor, pixels per square meter, was set from measurements of two different cylinders with known area. Matlab scripts for the frontal area measurements are included in appendix B.

(a) **(b)**

Figure 3.5: Light settings for the frontal area measurements. Picture (a) taken at the start of the measurement and picture (b) at the end of the measurement.

A threshold was set to a pixel value of 30 to be sure that none of the pixels on the test subject would turn up white. Some unwanted regions in the picture turned up black and were cut out of the picture afterwards. The region around the test subject's legs was also too dark and were cut out of all pictures. The pictures before and after cutting out the unwanted black regions is shown in Figure 3.6.

(a) **(b)**

Figure 3.6: Picture from Figure 3.5 (b) made binary with a pixel threshold of 30. Picture (a) before and (b) after cutting out unwanted black regions.

The frontal area in the region around the test subject's legs was computed by manually marking the region in 20 different pictures. The average area from the 20 pictures was added to the frontal area of the picture illustrated in picture (b) in Figure 3.6. The uncertainty of the area measurements was calculated to be $\pm 0.012\text{m}^2$ by using the root mean square error from nine pictures in the exact same position.

3.3 Blockage Correction

Maskell suggested the equation

$$\left(\frac{C_{du}}{C_{dc}}\right) = 1 + \theta C_{du}\left(\frac{A}{S}\right), \tag{3.1}$$

for estimating the wake blockage in a closed wind tunnel [13]. C_{du} is the uncorrected drag coefficient, C_{dc} is the fully corrected drag coefficient, A is the projected frontal area area of the object, S is the area of the cross section of the wind tunnel and θ is the blockage constant. The blockage constant is an empirical constant and it is determined by the base pressure coefficient and the aspect ratio [13]. The blockage constant was then estimated to be

$$\theta = 0.96 + 1.94e^{-0.06AR}. \tag{3.2}$$

These assumptions were made on flat-plates and the assumption was shown to be valid for $A/S < 0.21$ and it was also shown that the correction was valid for plates mounted to the floor as long as the plate had twice the height reflected on the floor as a plane of symmetry [13]. When testing humans a cylinder shape will be a better assumption than a flat plate. For a surface ratio up to around 10% the Maskell theory has shown to be accurate also for cylinders [14].

For the blockage correction Maskell's method was used. The cross section of the wind tunnel is $S = 4.86m^2$ and the frontal area of the test subjects in the experiments were $A < 0.7m^2$. This yields that $A/S < 0.14$, so Maskell's method should be a good estimate when testing humans. The blockage constant was determined by using equation (3.2). In this experiment the aspect ratio of a human body was determine to be $AR = 3$, which gives $\theta = 2.58$. Rearranging equation (3.1) and inserting the value for θ, the corrected drag coefficient becomes

$$C_{dc} = \frac{C_{du}}{1 + 2.58C_{du}(A/4.86m^2)}.$$

3.4 Test Subjects and Experiments

Three different experiments were performed for this thesis and the raw data in all experiments are presented in appendix C. The first experiment ($E1$) was a preliminary experiment. The first test subject ($TS1$) had no experience from competitive alpine skiing. In this experiment measurements on arm adduction and abduction as well as elbow flexion and extension were made. In the second experiment ($E2$), the test subject ($TS2$) was a female from the Norwegian world cup alpine team. A whole range of body positions was captured. The first draft of the complete model was made from this experiment, as this was the first experiment where a complete full range of positions was tested on one test subject. Results from the two first experiments are presented in chapter 4. The third experiment ($E3$) included four test subjects ($TS3, TS4, TS5$ and $TS6$) all professional athletes from Norwegian national team. The goal of this experiment was to find a correlation between C_DA and different body shapes. The goal was then to make a model that could be used for all athletes with as few changes to the model as possible. The results are presented together with the model in chapter 5.

The C_DA value depends both on the frontal area and the shape of the object as mentioned in section 2.1.1. Both the C_DA and the frontal area were measured and the C_DA values are used in the final model as it was considered to be more handy when the model was going to be used out in the field. Otherwise two models has to be made, one for the projected frontal area and one for the drag coefficient. All measurements that the model is based on were performed without poles. This was done in order to get more accurate results, considering the uncertainty of how a small change in the angles of the pole would affect both the drag coefficient and the frontal area. Measurement with and without poles were also performed to see what kind of effect the poles had. This was done in both the reference position with the poles straight down and in a hockey position, as shown in Figure 3.3. The difference with and without poles was in both cases in the range $\pm 1.5\%$, which is lower than the uncertainty of the measurements. Hence the changes in drag possibly made by the poles were neglected in this thesis.

Chapter 4

Experimental Results and Discussion

4.1 Hip-Knee Motion

The raw data for the hip-knee motion, from the measurements on $TS2$, is represented in Table C.3 in appendix C. The C_DA value for the reference position (at 100%) was measured to 0.412m^2, after taking account of the blockage correction. The tendency of the results and the measured points are illustrated in Figure 4.1.

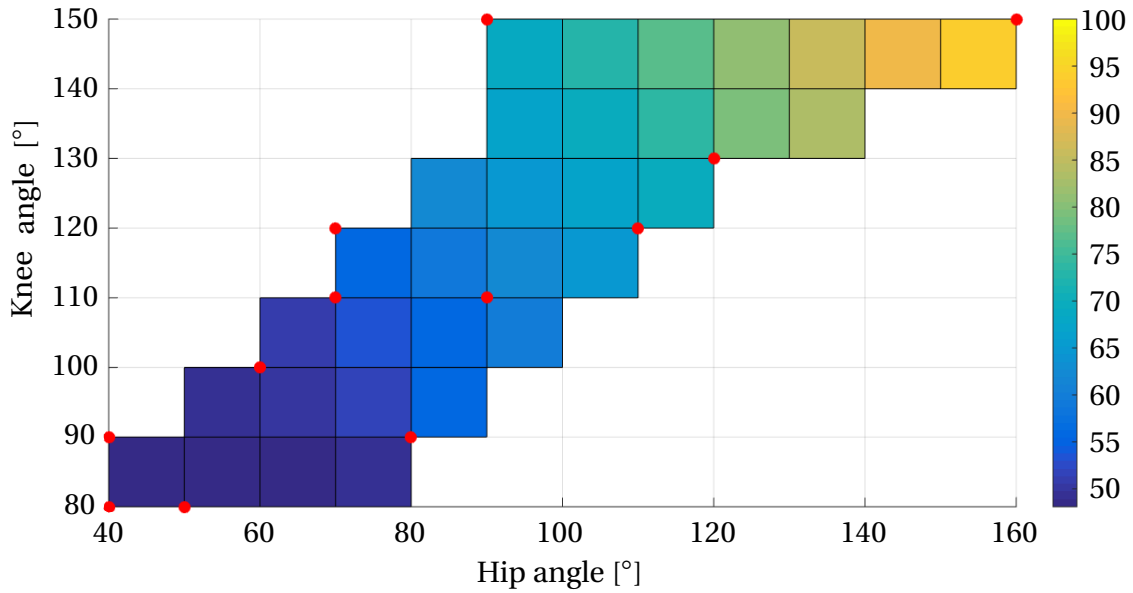

Figure 4.1: Percentage C_DA relative the reference position at the different knee and hip angles measured on $TS2$. The color bar shows the percentage C_DA and the measured points in the experiment are presented with red dots.

An observation from this result is that both the hip angle and the knee angle give a relative constant slope of C_DA for hip flexion with angles ≥90° and a relative constant, but smaller slope for hip flexion with angles ≤90°. The same tendency was observed in the authors project work [12], but with steeper slopes in both the hip-direction and the knee-direction. However, in the authors project work [12] the blockage correction was not taken into account and since

$$C_{dc} \sim \frac{C_{du}}{1 + \alpha C_{du} A},$$

the relative differences will be greater, especially when the frontal area A is large. The change in C_D range from 100% in the reference position to 76.9% at the lowest position, the uncertainty in C_D was calculated to be ±3.4% by the root mean square error, from the same nine measurements as for the uncertainty in the frontal area measurements. The frontal area range from 100% to 58.2% with an uncertainty of ±2.1%.

This means that the change in the frontal area has a greater contribution to the change in C_DA than the C_D.This can explain why the change in C_DA is greater for the hip angles ≥90°. A big part of the frontal area of a human body is from the hip and up to the shoulders, and by moving the hip down to an angle of 90° this area is reduced.

4.2 Arm Angle

The result from the arm angle experiment shows percentage change with respect to the reference position of the arms, an arm angle of 90°. The raw data from the experiments and the different knee and hip angles are presented and described in section C.1 and C.2 in appendix C. The results are shown in Figure 4.2. For the arm angle, the frontal area was first assumed to be constant for arm angle ≥0°, but as shown in appendix C, this was not the case due to movement of the test subject. Therefore, to get the real change in C_DA, the C_D values are calculated for each measurement and the C_DA values are computed with the area from the reference position (arm angle 90°) for all arm angles ≥0°.

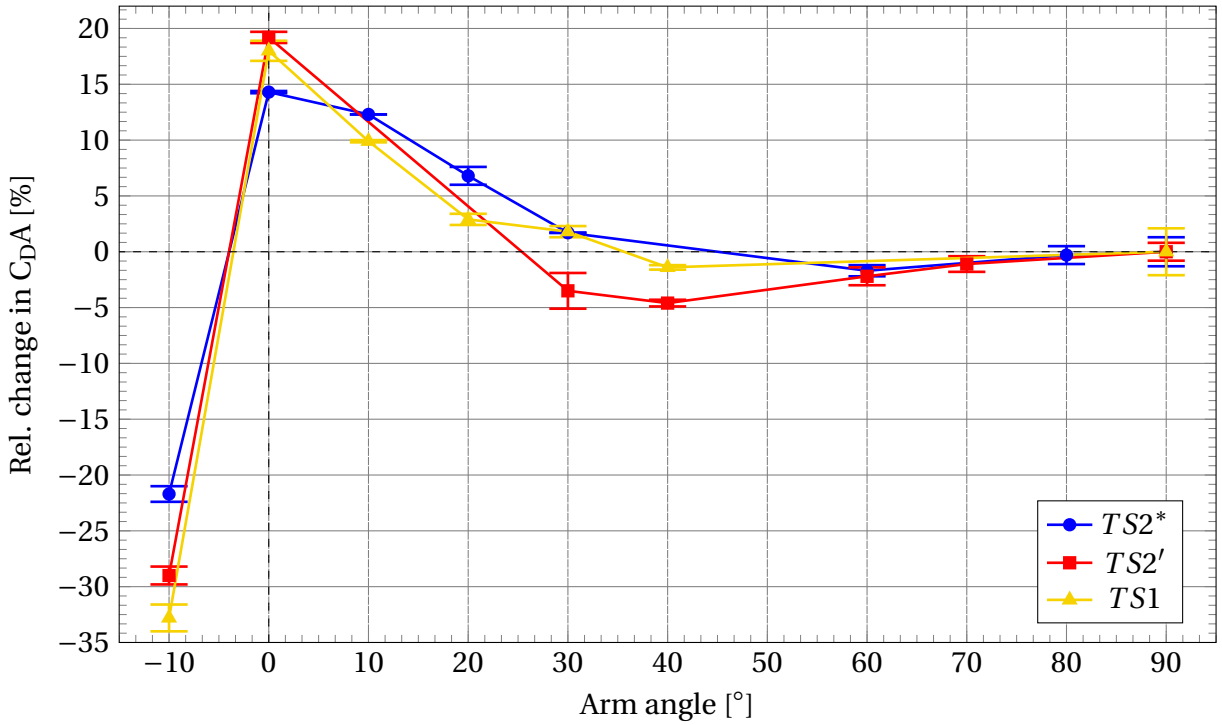

Figure 4.2: Percentage change of the C_DA values, relative to the reference position, as a function of the arm angle. When the arms are placed in front of the body of the test subject, the arm angle is defined as -10°.

$TS2'$ and $TS2^*$ are both measurements done on $TS2$ with different knee and hip angles, explained in appendix C. The most interesting results from these experiments may be from the arm angle. It had been assumed by NSF and others that the drag force was smaller with an arm angle of 0° than an arm angle ≥0°. For example, a typical flight position where the skier is as compact as possible with an arm angle of 0°, shown in Figure 4.3, is assumed to be a good aerodynamic position. This is a flight position widely used in downhill and Super-G.

Figure 4.3: Classical flight position for an alpine skier with arms along the torso. Foto: Scanpix.

The change in the region between 30° and 0° may be explained by the theory of interacting cylinders in section 2.3. Both the arms and the upper body can be modeled as cylinders and when the arm angle is in the range of 0° to 30° the arms are interacting with the upper body. In the upright position the arms and upper body are interacting as side-by-side configuration and as a staggered configuration when the hip angle is ≤150°. However, to find an exact position where the arms start to interact with the upper body is difficult as the diameter is not the same for the upper and lower body and smaller than the diameter of the upper body.

In the region from 0° to 90°, the frontal area is assumed to be constant, and the change in C_DA should then be explained by the change in C_D. By looking at the raw data in appendix C one can see that there is a small change in C_D from 90° to 30°. The change in C_DA in this region can mostly be explained by uncertainty in measurements, but also by a small change in C_D that can come from a small change in the position. In some of the measurements test subject $TS2$ assumed lower position and this changed the C_D. For the measurement at arm angle 0° the frontal area was smaller than for the reference position, this may be because some parts of the arms get in front of the upper body, making the frontal area smaller. This is not affecting the C_DA directly as a constant frontal area was used, but this can affect the correction values of C_D.

As expected, the C_DA values for arms inside the body are lower, and from the raw data one can see that this is both because of the frontal area and the drag coefficient. The C_DA values for $TS2'$ and $TS1$ are lower than for $TS2^*$ which is expected as the percentage change in frontal area is greater when the test subject is standing in a lower position.

4.3 Elbow Angle

The results from the elbow angle experiment show percentage relative change with respect to the reference position of the elbows, an elbow angle of 180°. The raw data from the experiments and the different positions of the knee, hip and arm angles are presented and described in section C.1 and C.2 in appendix C.

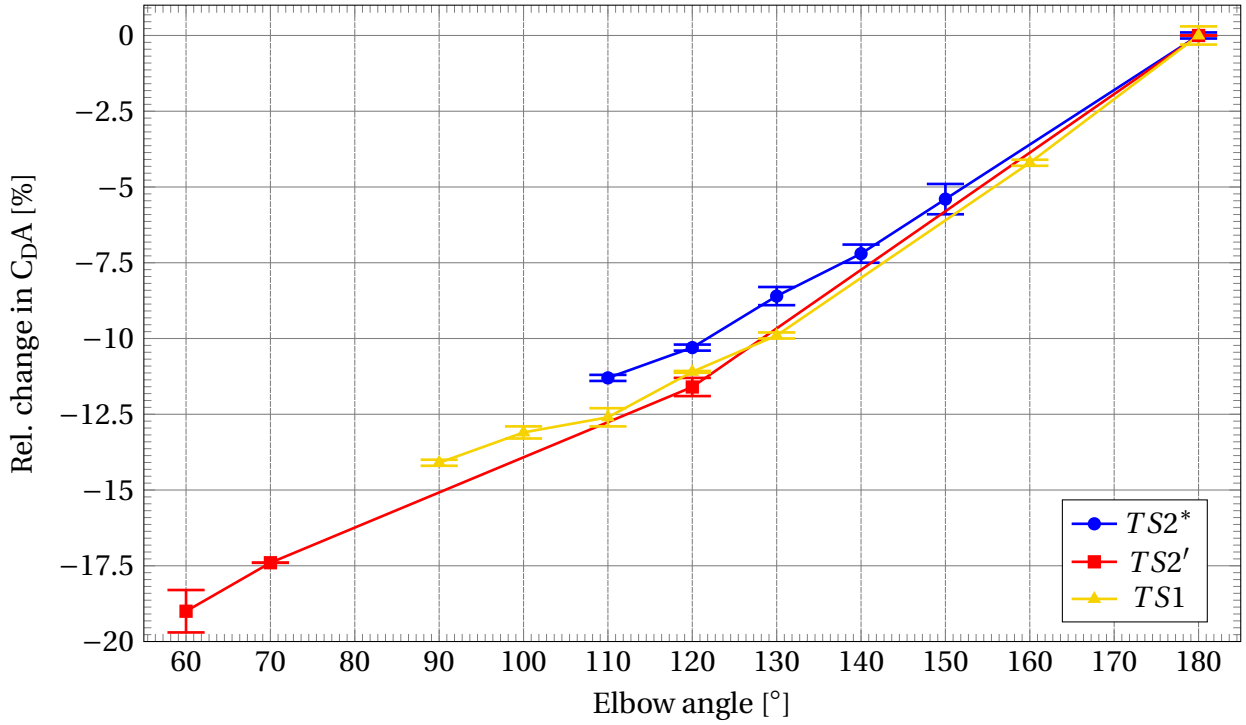

Figure 4.4: Percentage change of the C_DA values, relative to the reference position, as a function of the elbow angle.

For $TS2$ there seems to be little change in the drag coefficient from the reference position with an elbow angle of 180°, so the change appears to come from the change of the frontal area. The area of the arms from the elbow and out to the hands was calculated to be 0.076m^2. In the upright position, in measurement $TS2^*$, this yields a change in frontal area of 13.6% and 22.2% in the measurement of $TS2'$. The measurement on $TS1$ is more uncertain as $TS1$ was instructed to keep an arm angle of 0°, but after analyzing the pictures the arm angle was ~ 20° and a small change in the arm angle in this region can make a big difference in C_D.

4.4 Flight Position

As mentioned in section 4.2, one of the most interesting results from these experiments is how the drag is increasing when the arm angle approaches zero. This will not only affect the flight position visualized in Figure 4.3, but also the flight position in Figure 4.5. The flight position with the arms behind the legs, as shown in Figure 4.5, is assumed to be the second best flight position behind the hockey position. The problem with this position is that the skier has to move the arms along the side of the body, with an arm angle ~0°, to get to this position. This happens twice as the skier wants to get back to the hockey position after the flight.

Figure 4.5: Flight position for an alpine skier with hands behind the legs. Foto: GEPA Pictures.

In experiment $E3$ test subject $TS6$ was tested in four different possible flight positions. This was done to get knowledge of C_DA in different flight positions. In all four positions the knee and hip angle were kept constant, the four test positions were:

1. Flight position shown in Figure 4.5.
2. Flight position shown in Figure 4.3.
3. Flight position with arm angles 45° and elbow angles 180°.
4. Flight position with arm angles 90° and elbow angles 90°, shown in Figure 4.6.

The results from the flight position experiment are shown in Table 4.1. Positions 2, 3 and 4 were compared to 1 as position 1 was assumed to be the one with the lowest drag.

Table 4.1: Data from four different flight positions tested on test subject *TS*6.

Position	A [m^2]	Change [%]	C_D [ ]	Change [%]	C_DA [m^2]	Change [%]
1	0.373	0	0.520	0	0.194	0
2	0.416	12.0	0.732	40.9	0.305	57.1
3	0.422	13.0	0.589	13.3	0.248	28.1
4	0.386	3.6	0.554	6.6	0.214	10.4

An alpine skier will always try to maintain a good hockey position. The goal of this experiment was to find the best possible flight position when the hockey position is not an option. Therefore the hockey position was not tested in this part of the experiment. As expected, flight position 2 with the arms straight down along the side of the body yields a high C_DA value. When a skier has the arms behind the legs, like position 1, the skier is reducing the frontal area by hiding the hands, the same effect will appear in position 4. After consulting with the test subjects in *E*3, it may be hard to keep the arms with an elbow angle of 90° as shown in Figure 4.6, but theoretically this is a good position. The advantage with position 3 and 4 is that the skier does not have to use position 2 to get to these two position. For a short flight time a better solution may be to use position 3 instead of using position 1 and 2.

Figure 4.6: Picture from measurement of flight position 4 tested by *TS*6.

Another aspect with a flight position that should be considered is the distance between the legs. As mentioned in section 2.3, the distance between the center of two cylinders should at least be twice the diameter of the cylinders in order to keep the drag coefficient low. The width of an alpine boot is ~13cm, so the the distance between the legs should be 26cm or more. When gliding on snow the distance between the legs is in the same range as the shoulder width ≥30cm, which makes the aerodynamics of each leg independent of the other. In a flight position as shown in both Figure 4.3 and Figure 4.5 the distance between the legs is in the range where the the drag increases.

4.5 Turning Position

The aerodynamic drag through a turning position was investigated. In a turn, an alpine skier wants to turn as smoothly as possible from one direction to another to keep control of the center of mass and to try to avoid losing velocity through the turn. This is done by adjusting the knee angles as shown in Figure 4.7, the alpine skier is then keeping both skis on the snow at all time and has most of the pressure on the outside ski. A steeper slope, sharper turn or higher velocity yields a bigger difference in the knee angles.

Figure 4.7: An alpine skier in a turning position, with difference in right and left knee angle. Foto: GEPA Pictures.

The experiments with the different knee angles were done by replacing the left alpine binding on the force balance with an adjustable front binding. First measurements were made in two positions, position 1 was the reference position and position 2 was a position with a high knee angle and a low hip angle. Measurements were then made with three different heights of the left leg. Results for both positions are presented in Table C.8 and C.9 in appendix C. The highest position for the left leg in position 2 is shown in Figure 4.8. The relative percentage change between the two positions with no difference in knee angles is plotted as a function of the difference between the right and left knee in Figure 4.9.

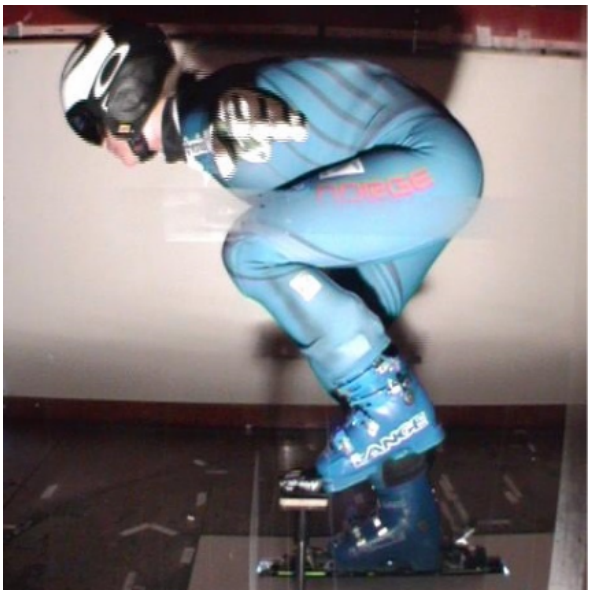

Figure 4.8: Measurement from the turning position experiment, with a low hip angle and the highest position tested for the left leg.

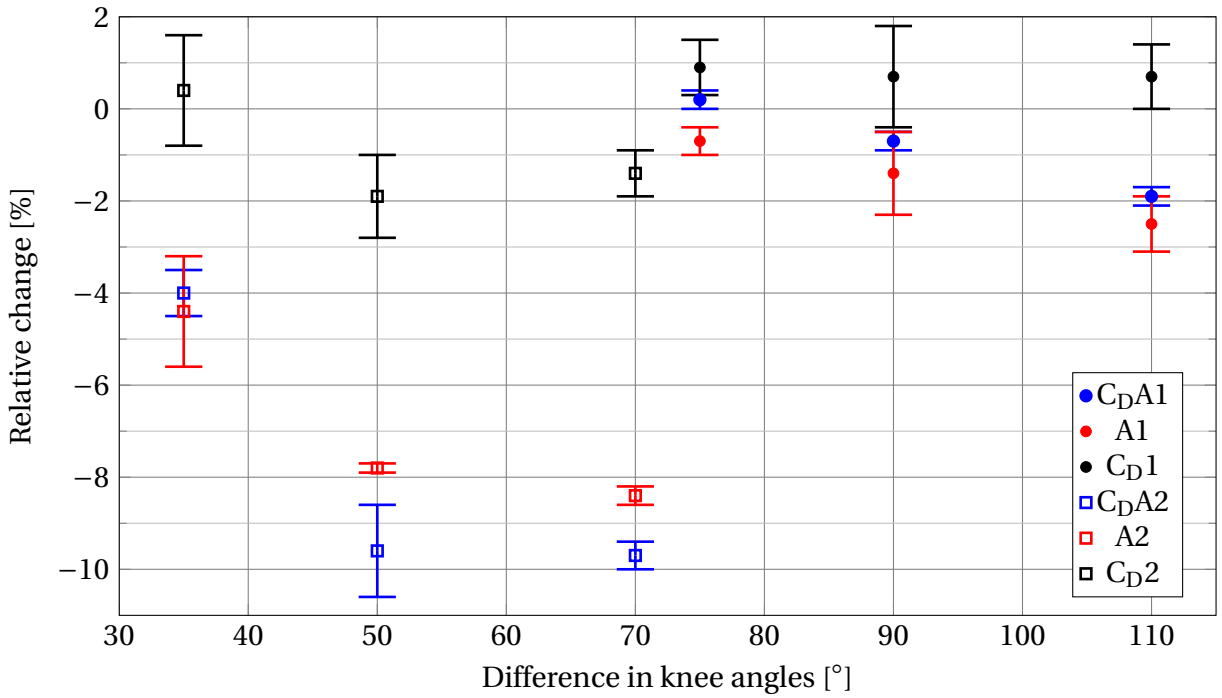

Figure 4.9: Percentage relative change for position 1 and position 2 with respect to no difference in knee angle. Round markers indicate position 1 and squares position 2. The positions are presented in appendix C.

Both in position 1 and position 2 the C_D is relatively constant, thus the changes in C_DA come from the change in frontal area when reducing one knee angle. The changes in both frontal area and in the C_DA is bigger in position two. This makes sense as the frontal area in this position is smaller, and that makes the relative change in the frontal area bigger when reducing one knee angle. C_DA seems to be reduced by the reduction of the frontal area when reducing one knee angle.

Even though the tendency is clear, the effect of different knee angles was neglected in the model for this thesis. To get a complete understanding of the effect, more measurements are needed. Due to time constraints in all experiments, this was not prioritized. The measurements of the turning position will anyhow not be accurate when investigated like described above, because this method does not take into account the ground effects in a turn. When a skier is turning a large percentage of the body will be close to the ground, and this will affect the drag force. This has to be investigated further and validated in the field to study ground effects before being implemented in the model.

Chapter 5

Model Description and Validation

5.1 Description

The script for the model computing the C_DA values based on the body position is shown in appendix E and visualized in a flow chart in Figure 5.1.

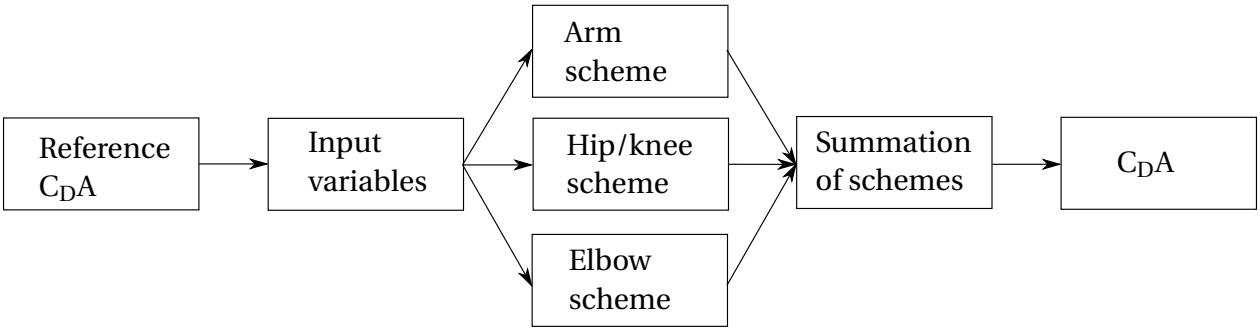

Figure 5.1: Flowchart describing the model computing C_DA based on body position. Where the C_DA in the reference position has to be defined and uses hip angle, knee angle, right and left arm angle and right and left elbow angle as inputs to compute a C_DA value.

The model is based on of three different regression schemes made from the results from the hip-knee motion, arm angle and elbow angle experiments. The three different schemes are explained and visualized below. The model is based on percentage change in C_DA, so the C_DA value in the reference position must be defined first either from wind tunnel measurements or from a separate model.

The input variables are the knee angle, hip angle, right and left arm angles and right and left elbow angles. The hip-knee scheme compute a percentage C_DA, relative to the reference position defined. For the results in this thesis with $TS2$ the hip-knee scheme will compute a number between 100 in the highest position and 47 in the lowest position. The arm and elbow angles are then used to compute the relative percentage change in the right and left arm and elbow, this is added or subtracted from the value computed by the hip-knee scheme. The arms and elbows were assumed independent of each other, therefore it was assumed that the right and left arm and elbow each contributed with half of the change in the C_DA. The model can also easily be modified with new results or other input variables.

5.1.1 Hip-Knee Scheme

Based on the results from the hip-knee motion the slope in both the knee angle-direction and the change in the hip angle-direction was assumed to be constant for hip angles greater than 90°. The same was found for hip angles smaller than 90°, but with another slope. The regression model was therefore split in two parts, one regression for hip angle smaller than 90° and one for hip angle greater than 90°. The hip-knee model is shown in Figure 5.2.

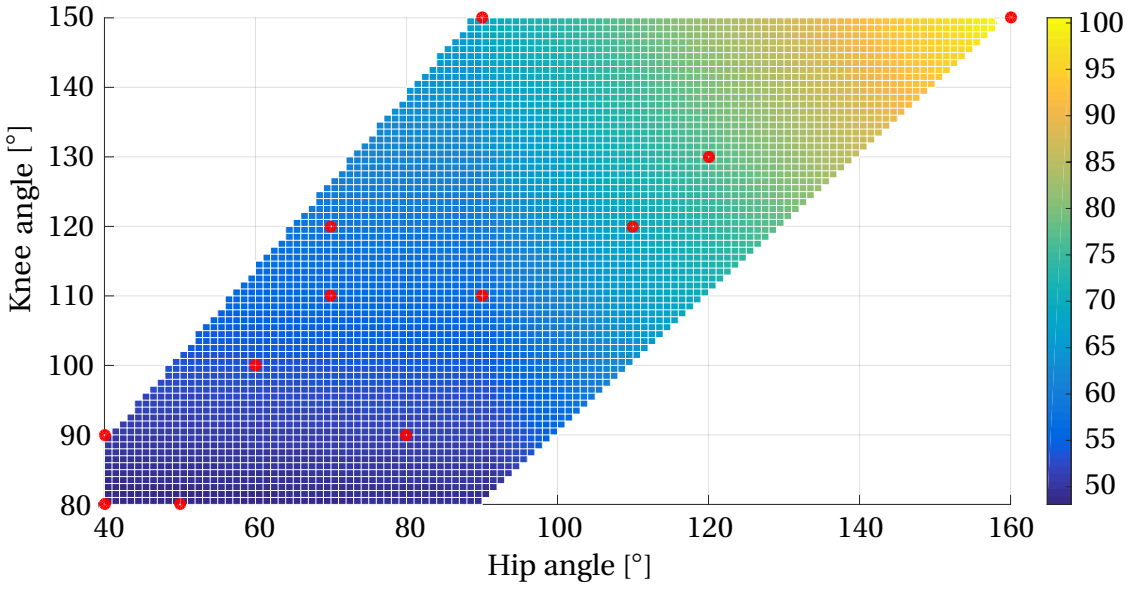

Figure 5.2: Regression model for the percentage C_DA relative the reference position for all hip and knee angles. The color bar shows the percentage C_DA and the measured points in the experiment are presented with red dots.

The regression equation used was

$$C_d A_{corr} = C_d A_{ref} + h_x dx + h_y dy,$$

where C_dA_{corr} is the computed value, C_dA_{ref} is the reference value in the highest position for hip angles above 90° and lowest position below 90°, h_x is the step length from C_dA_{ref} in x-direction, h_y the step length from C_dA_{ref} in y-direction, dx the angle change in x-direction and dy the angle change in y-direction. One way to illustrate the sufficiency of a fitted regression model is by the coefficient of determination R^2 [15]. R^2 is the proportion of variability, a value between 0 and 1, explained by the fitted model and is defined as

$$R^2 = \frac{SSR}{SST} = \frac{\sum_{i=1}^{n}(\hat{y}_i - \bar{y})^2}{\sum_{i=1}^{n}(y_i - \bar{y})^2}, \tag{5.1}$$

where SSR is the sum of squares due to regression, SST is the total sum of squares, $\bar{y}$ the mean value of the observed data, y_i the observed data and $\hat{y}_i$ data point from the regression model [15]. The coefficient of determination for the hip-knee scheme was determined to $R^2 = 0.982$.

5.1.2 Arm Scheme

The arm scheme is plotted in Figure 5.3 together with the measured points.

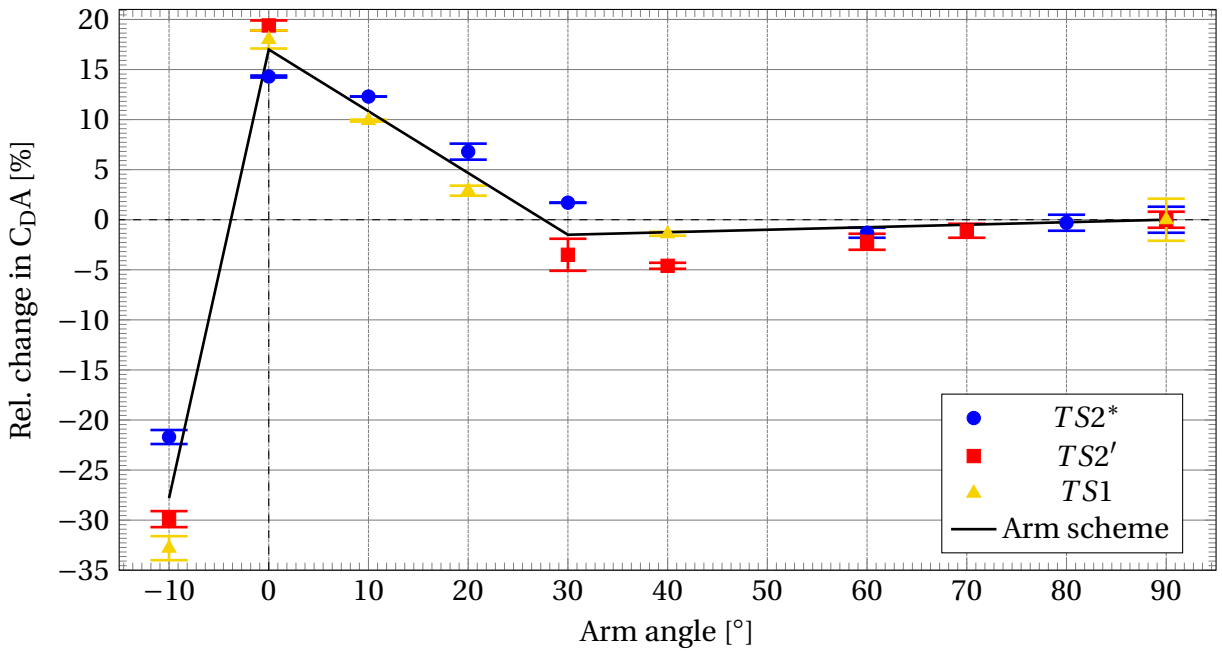

Figure 5.3: Regression model for the percentage change in C_DA relative an arm angle of 90°, together with the measured points from Figure 4.2.

The regression of the arm angle was divided into three different regions where the percentage rate of change of C_DA was assumed constant. The first region was from −10° to 0°, arms inside the body outline. The second region was an arm angle from 0° to 30° and the last from 30° to 90°. The regression was made in the same way as shown in Figure 4.2, percentage change in C_DA from the reference position of arm angle 90°. The regression equation used was

$$C_d A_{\%corr} = C_d A_{\%ref} + h_x dy, \tag{5.2}$$

Where $C_dA_{\%corr}$ is the computed percentage change from an arm angle of 90°, $C_dA_{\%ref}$ starting point in the three regions, h_x the step length from the starting point and dy the angle change in y-direction. The coefficient of determination was calculated with equation 5.1 to $R^2 = 0.953$.

5.1.3 Elbow Scheme

The regression model for the elbow angle was divided into two different regions where the percentage change in C_DA was assumed constant. The first region was from 180° to 120°, the second region was an elbow angle from 120° to 60°. The elbow scheme is plotted in Figure 5.4 together with the measured points from the results.

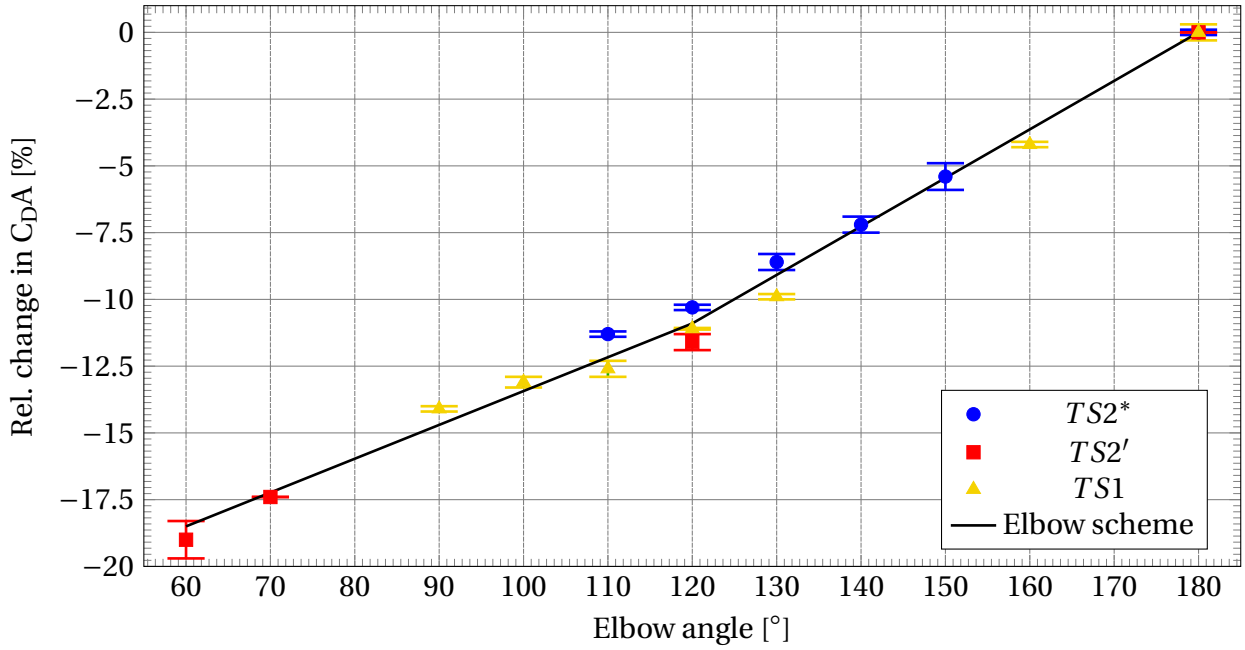

Figure 5.4: Regression model for the percentage change in C_DA relative to an elbow angle of 180°, together with the measured points from Figure 4.4.

Equation 5.2 was also used to compute the elbow angle scheme. The coefficient of determination for the elbow scheme was calculated with equation 5.1 to $R^2 = 0.993$.

5.2 Validation

To validate the model, three different test positions were chosen. The angles in the knee, hip and arms were chosen randomly and three measurements were made in each position. In this validation the elbow angles were chosen to remain constant at 180°. This was done to get a more accurate result, because the elbow angle was hard to determine from the picture taken. The percentage differences between the modelled result and the measured result are shown in Figure 5.5. The three test positions and the results are also presented in Table C.10 in appendix C. An error of ±2% is in the range of the expected error of the hip-knee scheme and the arm scheme, thus the model seems to be a good fit for the three validation positions. The third test position is shown as an example in Figure 5.6.

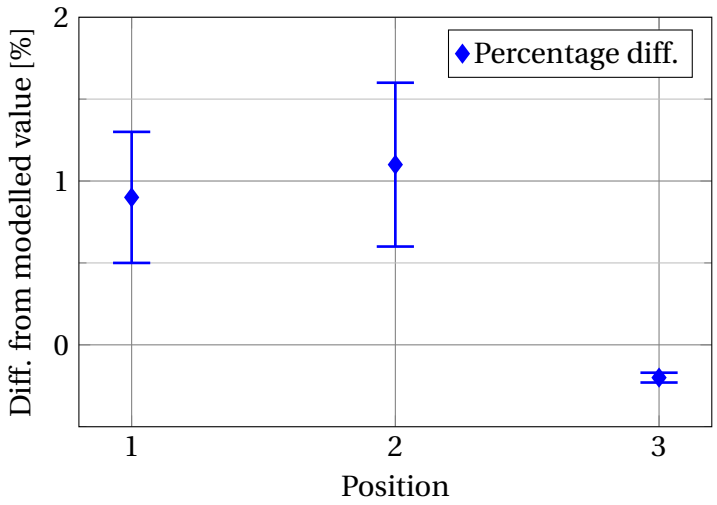

Figure 5.5: Percentage difference between the C_DA from the experiment and the model for the three validation positions, with the error bars from the measured points.

(a)

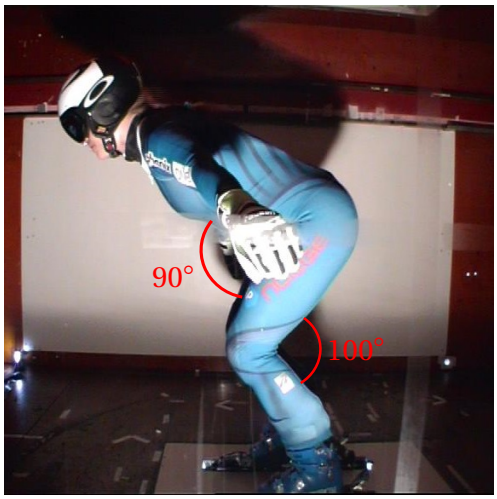

(b)

Figure 5.6: The third test position for validation, 100° knee angle, 90° hip angle, 60° left arm angle, 40° right arm angle and 180° for both elbow angles.

The elbow scheme was as mentioned not validated for $TS1$, but the results from section 4.4 can be used as validation. Test subject $TS6$ tested one flight position with an arm angle of 45° and elbow angle 180° (position 3 in Table 4.1) and one position with an arm angle of 90° and elbow angle 90° (position 4 in Table 4.1), shown in Figure 5.7 (b) and (c). The arm angles are not the same in these two positions, but the difference in C_DA from 90° to 45° in the arm scheme is -1.4%. Position 4 has a 13.7% smaller C_DA value than position 4 in Table 4.1, this yields that 12.3% of the change should come from the change in elbow angle. The elbow scheme estimates a -14.7% change in C_DA with an elbow angle of 90°, which is a little more than the difference for $TS6$. By looking at Figure 4.6 and Figure 5.7 (c), $TS6$ is not holding the lower arms horizontally as intended and this could also have an effect on the results.

In the same way as for the elbows, the arms scheme can be validated by looking at the flight positions in Table 4.1. The only difference between position 2 and 3 is the arm angles. Position 2 has arm angles of 0° and position 3 arm angles of 45°, shown in Figure 5.7 (a) and (b). The difference in C_DA between these two positions is 23% and the difference from the modelled C_DA is 18.5%, which yields a difference between the experimental results and the model of 4.5%. All measurements in the flight position were made with poles. As mentioned previously, the effect of poles was neglected in the model, but this could have affected the results in the range ±1.5%. Although the arm and elbow angles were validated on other test subjects, they indicate that the uncertainty of the model is in the range of ±4%.

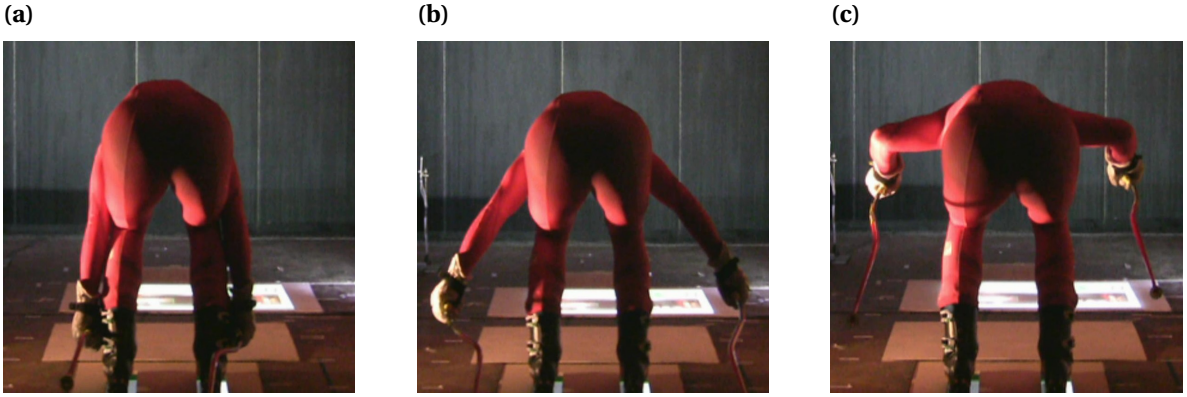

Figure 5.7: Back picture of flight position 2 (a), flight position 3 (b) and flight position 4 (c) from Table 4.1, used as an validation of the arms and elbows for the model.

5.3 Individual Adjustments

The model described in 5.1 is based on only two test subjects. The goal of experiment $E3$ was to determine how both the drag coefficient,C_D, and the drag area, C_DA, are changing for different body shapes and sizes, and to use this information to find an individual adjustments to the model. Experiments were performed on four test subjects ($TS3$-$TS6$), and also the results from $TS2$ were compared to the other test subjects. Results from $TS1$ were not included, as those results only consist of arm and elbow measurements. The raw data from $E3$ is presented in appendix C.3.

The goal for the first part of experiment $E3$ was to see the percentage change in C_DA values from the reference position to the hockey position with arms to the side. The reference position in the model will always have the value of 100% in the hip-knee scheme. The lowest percentage value is wanted in the knee-hip scheme, as this is the starting position for the lower part (from hip angle 40° to 90°) of the scheme. The percentage value in the lowest position measured, relative to the individual reference position, for all test subjects are shown in Figure 5.8.

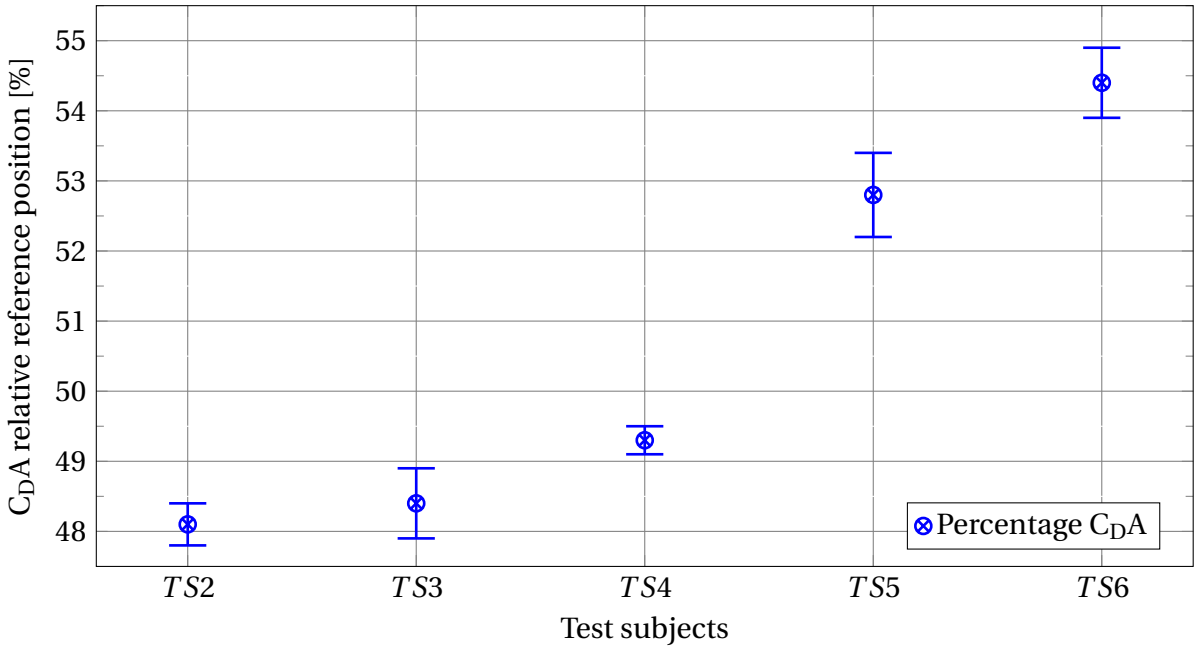

Figure 5.8: Percentage C_DA in the lowest position measured,relative reference position, for five different test subjects.

These results show that for test subjects $TS2$, $TS3$ and $TS4$ the percentage C_DA in the lowest position is in the same range, with just 1.2% difference from $TS4$ as the highest to $TS2$ as the lowest. The results for $TS5$ and $TS6$ are higher than the three others. The pictures from their measurements were studied and compared to $TS3$ and $TS4$, shown in Figure 5.9.

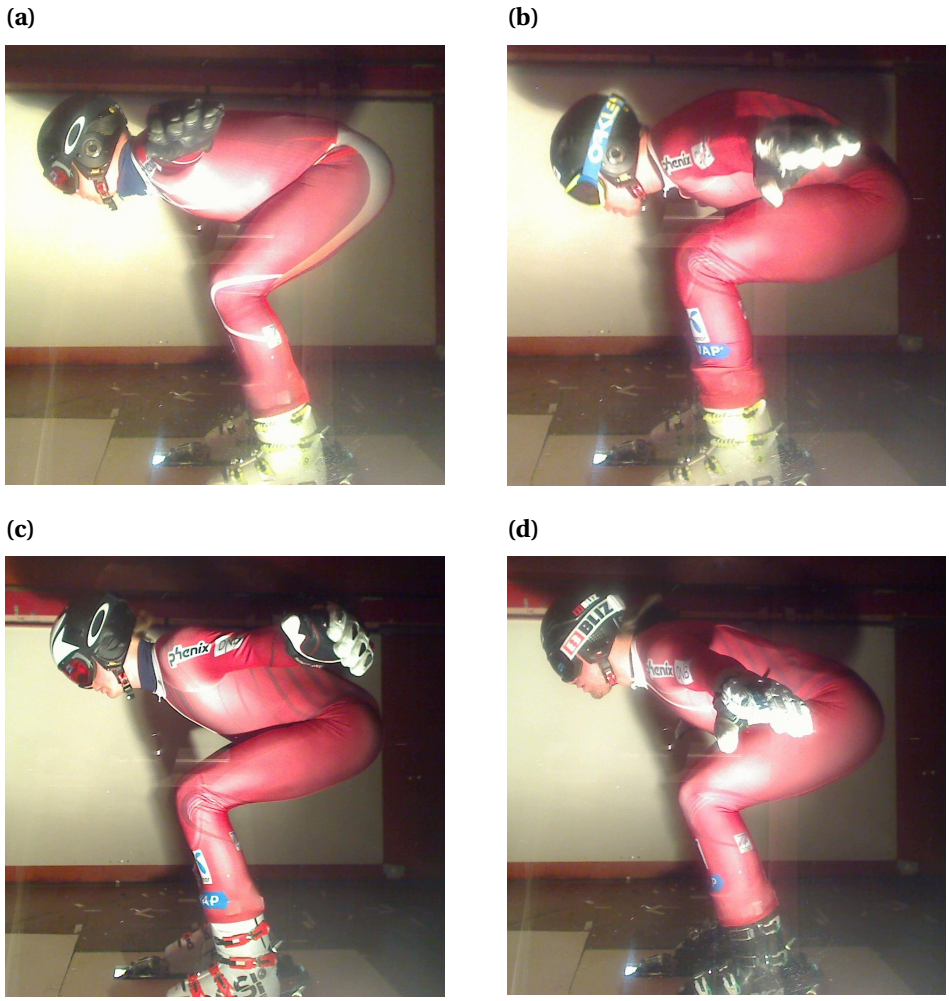

Figure 5.9: Side pictures, used to measure the knee and hip angle, from the measurements of the lowest positions measured on $TS3$ (a), $TS4$ (b), $TS5$ (c) and $TS6$ (d).

The hip angle in Figure 5.9 (c) and (d) are higher than in (a) and (b). A small change in the hip angle to a higher position will increase C_DA, as described in section 4.1. It was concluded that $TS5$ and $TS6$ did not hold the intended position. The angles in the knees and hips for both $TS5$ and $TS6$ were measured to be 90° and 70° respectively. The modelled C_DA for these angles was 53.4%, $TS5$ had a C_DA of 52.8% and $TS6$ had a C_DA of 54.4%. So even if the values in Figure 5.8 are high they are in the range of what is expected by the model.

With these results the change from the reference position to the lowest position appears to be close to constant with a value of 48.6% in the hockey position. This is the mean value for $TS2$, $TS3$ and $TS4$ in Figure 5.8. The results of $TS5$ and $TS6$ were neglected as they did not hold the intended position. However, the model matched the measured values in the position held by $TS5$ and $TS6$.

The change in the drag coefficient C_D was also investigated. Both the reference position and the hockey position, position 1 and 3 in appendix C.3, were tested for all test subjects and compared. The third position tested, position 2 in appendix C.3, was not used in this comparison as this position was different for the different test subjects. The mean C_D values for the reference position and the hockey position were calculated and the difference from the mean values in both positions are shown in Figure 5.10.

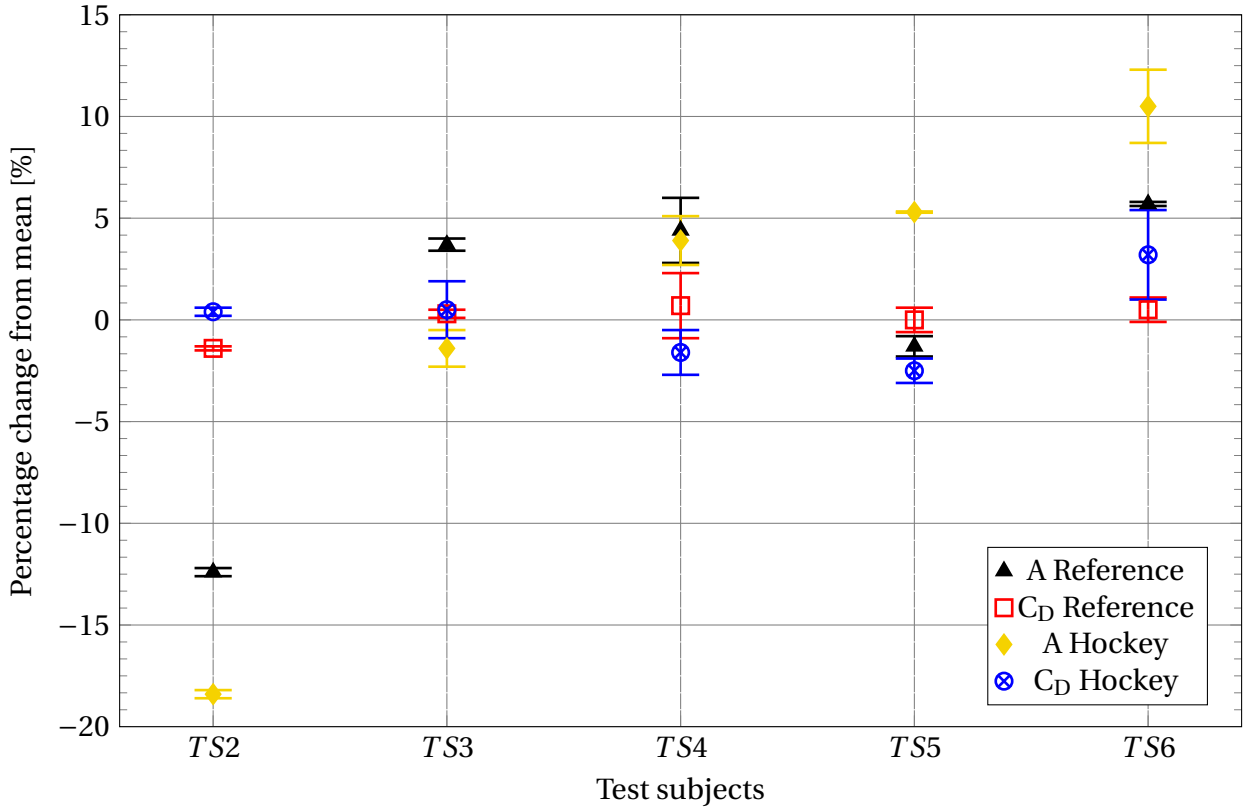

Figure 5.10: Percentage change, relative the mean value, from five different test subjects of frontal area and drag coefficient in reference and in hockey position. Mean values are shown in Table 5.11.

The mean values from both positions are shown in Table 5.11. Figure 5.10 shows the difference in frontal area from the biggest to the smallest test subject, but there is only a small change in the drag coefficient. The variation in both the frontal area and dag coefficient are greater for the hockey position. This was expected as both $TS5$ and $TS6$ stood in a higher position than intended, as described above.

Table 5.11: Mean values of frontal area and drag coefficient for test subjects $TS2$-$TS6$ in the reference position and the hockey position.

Position	A [m^2]	C_D [ ]
Reference	0.658	0.725
Hockey	0.442	0.548

An interesting result from this experiment is the small changes in the C_D for the different test subjects. In the reference position, $TS6$ has the biggest area and $TS2$ the smallest. The difference in frontal area is 17.1% and is visualized in Figure 5.12. Despite a big difference in frontal area, the biggest difference from the mean value of the drag coefficient is only 1.4%. This is in the range of the uncertainty of the frontal area measurements, so the drag coefficient was determined to be a constant value at C_D=0.725, the mean value of the test subjects. Anthropometric measurements of the test subjects are presented in appendix D. Based on these results it can be assumed that only the projected frontal area in the reference position is needed as individual input into the general model. With a constant percentage change from the reference position to the hockey position, no adjustments have to be made for the slopes in the model. The assumption that C_D is constant implies that the only variable that then has to be changed for individual adjustment is the frontal area of the test subject.

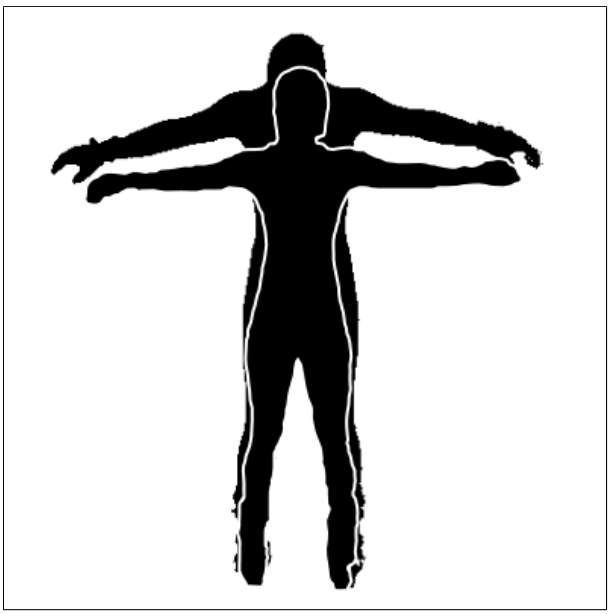

Figure 5.12: Visualization of the difference in frontal area of the smallest test subject, $TS2$, and the biggest, $TS6$, in the reference position.

In theory, if the only variable that has to be defined for a test subject is the frontal area, no wind tunnel measurements are needed for individual adjustment of the model.The final model was tested on four test subjects in experiment $E3$. All four test subjects were tested in three positions each. The test positions are presented in section C.3 in appendix C and are meant to represent the reference position, the hockey position and one position in the middle of the range of motion of the hip and knees. The modelled values are presented together with the measured values in appendix C, and the percentage difference from the experimental value to the modelled values are shown in Figure 5.13.

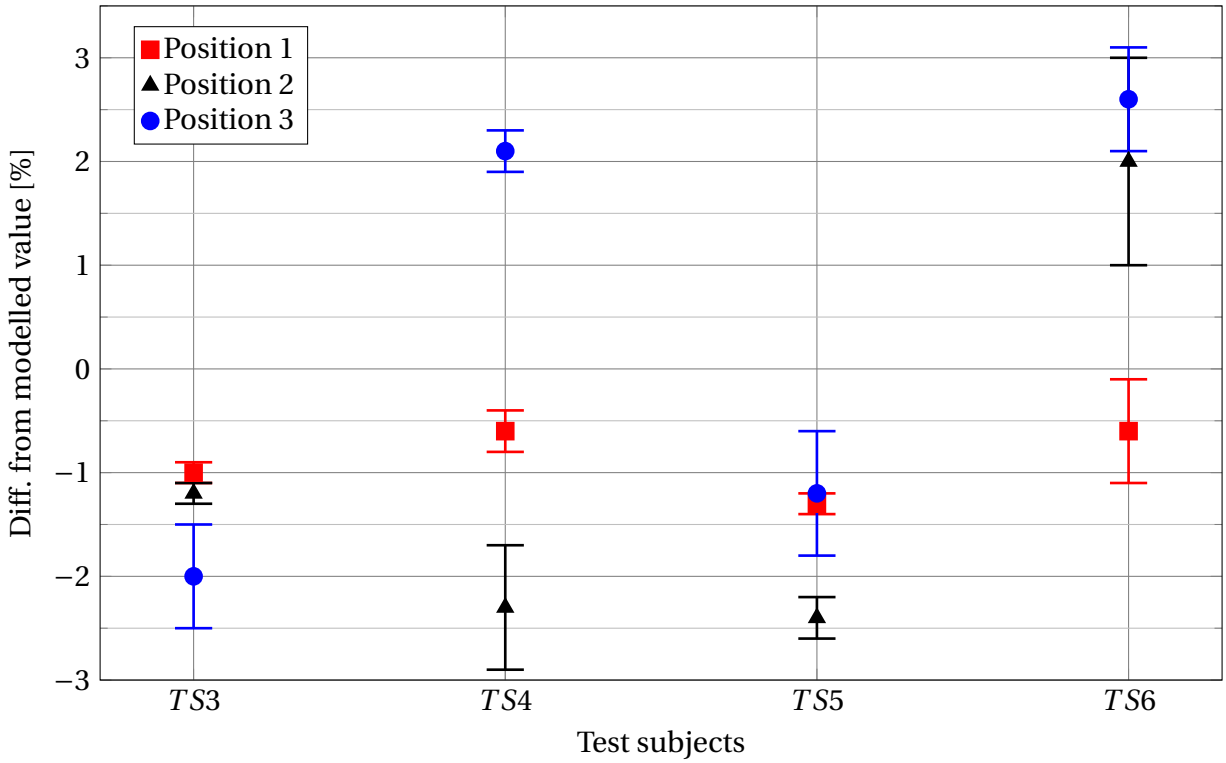

Figure 5.13: Percentage difference between the measured and the modelled C_DA in the three tested positions for $TS3$, $TS4$, $TS5$ and $TS6$, with error bars from the measurements.

As can be seen from Figure 5.13 all the experimental values lie in the range of ±3% of the values computed by the model. This should be in the range of the expected uncertainty of the experiments. The data set may be to small to conclude that the model is fitting with an uncertainty of ±3% in all positions, but the tendency is promising.

5.4 Field Results

If the model and the results from the experiments are going to be of any use for the NSF, the results from the wind tunnel and the numerical model have to be in accordance with results from the field. As mentioned, NSF uses a GPS-based system to calculate total breaking force on an alpine skier. To see the relation between measurements of the dGNSS and the results from the experiment and the model, measurements on test subject $TS6$ were made with the dGNSS in an alpine hill before experiment $E3$ was performed. As the dGNSS measures both the drag force and the ski-snow friction, measurements were made in a 18 meter flight section of the alpine course, as there is no ski-snow friction for an alpine skier during a flight. Measurements in three different flight positions were tested and the positions were later replicated in the wind tunnel.

Figure 5.14: Side picture of $TS6$ in position 1, the flight position with the hands hidden behind the legs.

The three flight positions tested were position 1, 2 and 3 from Table 4.1. Position 1 is the flight position with arms behind the legs, shown in Figure 5.14, position 2 is the flight position with the arms straight down on the side of the torso, shown in Figure 4.3 on page 21, and position 3 is the flight position with arm angles 45° and elbow angles 180°. As discussed in previous sections, and shown in Figure 5.14, the lower arms are hidden behind the legs in position 1. The measurements were taken as a time series of 0.6s from the middle of the flight. 18 time steps were used to calculate the mean values at each flight and the mean values are shown in Table C.19 in appendix C. Pictures from the time series in each position are shown on page 41.

Position1

Figure 5.15: Picture sequence from flight position 1 in the field experiment. Foto: NSF

Position2

Figure 5.16: Picture sequence from flight position 2 in the field experiment. Foto: NSF

Position3

Figure 5.17: Picture sequence from flight position 3 in the field experiment. Foto: NSF

For the modelling of position 1 the elbow angle was chosen to be 90°, as this should give the effect of hiding the lower arms behind the legs. When holding the arms as in position 1, the upper arms are held with an angle backwards which gives the upper arm a lower frontal area. In this case the upper arm was calculated to be 20% smaller due to this change, so the arm angle in the model was chosen to be -2° to compensate for this effect. The modelling of position 2 and 3 was done with input arguments 80° in the knees, 40° in the hip and 180° in the elbows and 0° in arm angles for position 2 and 45° for position 3. The relative change in both C_DA and the drag force with respect to position 1 are shown in Table 5.18.

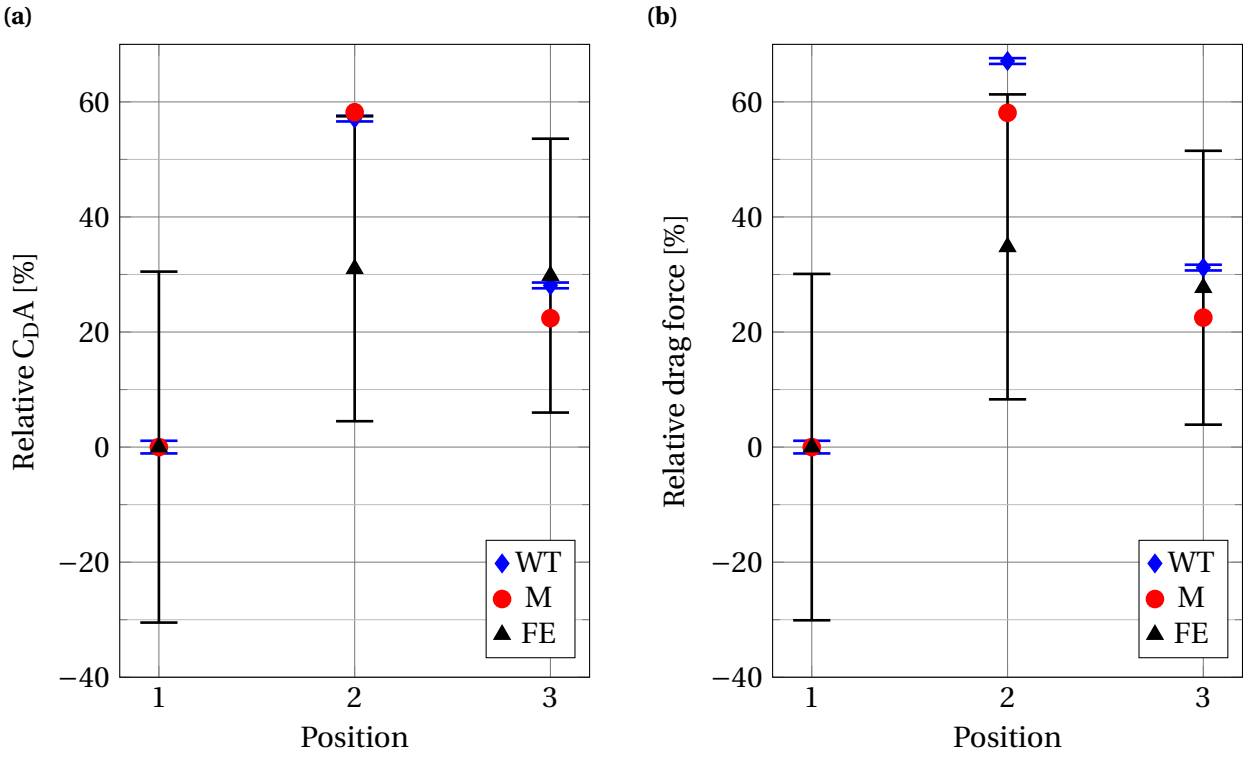

Figure 5.18: Relative change, with flight position 1 as a reference, for field experiment (FE), wind tunnel experiment (WT) and the numerical model (M). Numerical values are shown in Table 5.1.

The modelled force was estimated with the modelled C_DA and air density and velocity from the wind tunnel. In the field experiment, the velocity was measured in all three runs to be 32.5±0.5m/s and the air density was estimated to ρ=1.08kg/m^3.

Table 5.1 shows the C_DA values for the field experiment (FE), wind tunnel experiment (WT) and the numerical model (M). The results from the FE show that the C_DA values from position 1 and position 3 are higher than for measurements in the WT, but the relative change between position 1 and position 3 seems to be in the same range as for the FE. Position 2 is in the same range as the values from the WT.

Table 5.1: Numerical C_DA [m^2] values from WT, M and FE in the three position tested.

Position	1	2	3
WT	0.194	0.305	0.248
M	0.196	0.310	0.240
FE	0.227	0.297	0.295

By looking at the picture sequences and video from the flights, $TS6$ is more compact and kept position 2 better than position 1 and 3. For position 1, this flight may have been too short to get the complete benefit of moving the arms behind the legs. By looking at some of the first pictures in Figure 5.15, $TS6$ is still moving the arms along the body to maintain the intended position and this could have an effect on the results. For position 3, one can also see that $TS6$ is not as compact as in position 2. The fact that $TS6$ held the position best for position 2 may be because this was already a well known position for the test subject, as this position is used both in training and in competitions and is therefore a more comfortable position. Position 3 was new for $TS6$ before this experiment and that can make it more difficult to maintain.

Although the values from positions 1 and 3 were higher than in the WT, the results from this experiment looks promising, as they are in the range of the experiments from the WT and the M. The high value of position 1 can be explained by the movement of the arms when the test subject is getting to the intended position, and position 3 by a higher position in the upper body. An interesting result is to see the difference between positions 2 and 3. Even though $TS6$ has a higher position in the upper body in position 3, which should yield a higher C_DA, the C_DA is actually somewhat lower which may be a result of the change in arm angle from the change in arm angle.

Even though the tendency looks promising, it is hard to determine how well the M and WT corresponds to the FE. This because the uncertainty in the GPS-data from NSF is high, and because more measurements are needed for a complete understanding. Figure 5.19 shows the drag force measured through all 18 time steps of the flight.

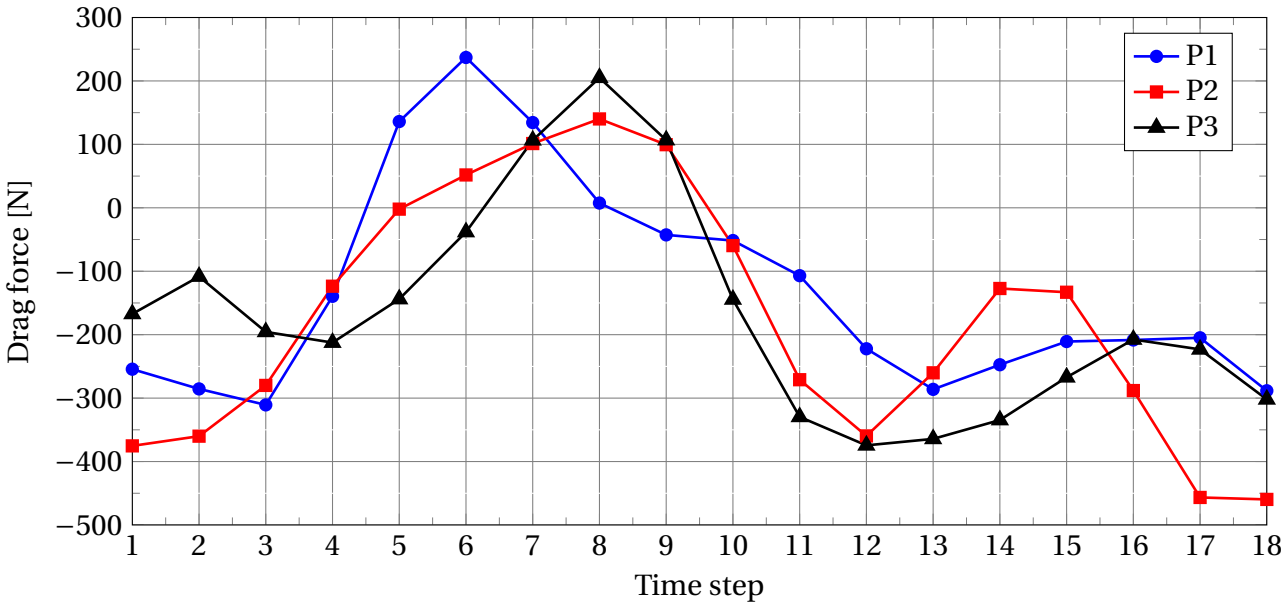

Figure 5.19: Drag force measured in the 18 time steps by the dGNSS in FE for positon 1 (P1), position 2 (P2) and position 3 (P3). Positive direction is defined as the direction of the velocity vector.

The dGNSS measures all forces acting on the skier and calculates the drag force by subtracting the gravitational force, thus assuming no other forces are at play. By studying at Figure 5.19, especially from time steps 4 to 10, some other forces are acting on the skier. This may be due to lift in some regions of the flight, something which is not accounted for by NSF and should therefore be investigated further. However, the tendency demonstrated by this experiment shows that the experimental data and the numerical model is in the range of what is expected in the field.

Chapter 6

Conclusion

This thesis has provided an overview of forces acting on an alpine skier. A complete database of how the C_DA is changing with respect to the different body segments used to explain a complete body motion in alpine skiing has been made. A numerical model that calculates the C_DA based on angles in different body segments has been introduced with an uncertainty of ±3%. A new method for calculating the frontal area inside a wind tunnel producing results with an uncertainty of $\pm 0.012 m^2$. Different flight positions were evaluated since the results from the change in arm angle showed that the aerodynamic drag increases when the arm angle approaches zero. The drag for different right and left knee angle was also briefly investigated, to replicate a turning position, and the change in C_DA seems to be proportional to the change in frontal area when ground effect is neglected.

The model was tested and validated on different test subjects and showed that the percentage relative change in C_DA from the highest to the lowest position was constant and that C_D was constant for different test subjects standing in the same position. The only parameter one then need to vary for personal adjustments of the numerical model is the frontal area of the test subjects in the reference position. By only changing this parameter, the model retained an uncertainty of ±3%. The results from the wind tunnel and the numerical model were compared to data from a preliminary field experiment, a flight sequence for one of the test subjects, and the results from the experiments in the wind tunnel and the numerical model were in accordance with results from the field experiment.

Chapter 7

Further Work

As the method for calculating the frontal area was developed and improved from experiment to experiment throughout this work, more iterations could help improve the method further. One such improvement could be to mount brighter lights in front of the test subject, as this would provide better contrast between the test subject and the surroundings. White plates could also be mounted on the floor around the test subject removing the need to crop the images around the legs. This should make the measurements both more accurate and efficient. The method should also be validated further by putting different objects of known area in the wind tunnel.

As mentioned, more measurements and perhaps an improvement should be made to the measurements of the turning position. With more and systematic measurements, the difference in knee angle can be used as an input in the model. This should also be validated and the ground effects has to be estimated in a turn to get a complete understanding. More measurement should also be done with and without poles in different positions to see if the assumption made in this thesis where the poles were neglected is a valid assumption, or if this should be an input in the model. Measurements with different suits used by NSF has not been tested in this thesis. The suits used by NSF are dependent both on the alpine disciplines and the weather conditions and the suits should therefore be tested and used as an input in the model. At the current time, the author has not found any similar work, and the results presented here should therefore be verified by an external source. More tests should also be done on more test subjects for a more complete validation of the model.

For a complete comparison of experimental data and field experiments, improvement of the methods used with the dGNSS should be done. For measurements in flight positions, lift should be taken into account for a more accurate estimate of the actual drag force. Measurements gliding on snow should also be done by neglecting an estimated snow friction. The dGNSS has to be tested on a test subject in the wind tunnel to see the effect the dGNSS has on an alpine skier. Tests should also be done with and without start number, as they are used both when training and competing. These measurements should also be done on more than one test subject for a more understanding.

As the model uses angles between body segments as input, some type of motion capture system has to be used. Without a motion capture system one can measure angles from pictures taken from small parts of an alpine hill, but this will be hard to manage for a complete race track of 3-4km. Both due to the man power one has to use, the time it will take and the amount of camera equipment one need to cover a complete alpine hill.

Bibliography

[1] M. Supej, L. Sætran, L. Oggiano, G. Ettema, N. Šarabon, B. Nemec, and H.C. Holmberg. Aerodynamic drag is not the major determinant of performance during giant slalom skiing at the elite level. *Scandinavian journal of medicine & science in sports*, 23(1):e38–e47, 2013.

[2] F. Meyer, D. Le Pelley, and F. Borrani. Aerodynamic drag modeling of alpine skiers performing giant slalom turns. *Medicine and science in sports and exercise*, 44(6):1109–1115, 2012.

[3] P. Kaps, W. Nachbauer, and M. Mössner. Determination of kinetic friction and drag area in alpine skiing. In *Skiing Trauma and Safety: Tenth Volume*. ASTM International, 1996.

[4] C. Barelle, A. Ruby, and M. Tavernier. Experimental model of the aerodynamic drag coefficient in alpine skiing. *Journal of applied biomechanics*, 20:167–176, 2004.

[5] D.A. Moldestad. *Some aspects of ski base sliding friction and ski base structure*. Fakultet for ingeniørvitenskap og teknologi, The Norwegian University of Science and Technology (NTNU), 1999.

[6] W. Nachbauer, P. Kaps, M. Hasler, and M. Mössner. Friction between ski and snow. In *The Engineering Approach to Winter Sports*, pages 17–32. Springer, 2016.

[7] M. Gilgien, J. Spörri, J. Chardonnens, J. Kröll, and E. Müller. Determination of external forces in alpine skiing using a differential global navigation satellite system. *Sensors*, 13(8): 9821–9835, 2013.

[8] M. Gilgien. *Characterisation of skiers' mechanics, course setting and terrain geomorphology in World Cup Alpine Skiing using global navigation satellite systems: injury risk, performance and methodological aspects*. The Norwegian School of Sport Science, 2014.

[9] M. Gilgien, J. Spörri, J. Chardonnens, J. Kröll, P. Limpach, and E. Müller. Determination of the centre of mass kinematics in alpine skiing using differential global navigation satellite systems. *Journal of sports sciences*, 33(9):960–969, 2015.

[10] D Sumner. Two circular cylinders in cross-flow: a review. *Journal of Fluids and Structures*, 26(6):849–899, 2010.

[11] P. Bradshaw. *Experimental fluid mechanics, second edition.* Pergamon Press, 1970.

[12] O. Elfmark. *Modelling of Forces in Alpine Skiing.* Project Work, NTNU, Trondheim, Norway, 2016.

[13] K. Cooper. Bluff-body blockage corrections in closed-and open-test-section wind tunnels. *Wind Tunnel Wall Correction (AGARD-AG-336), BFR Ewald, ed., Advisory Group for Aerospace Research and Development, North Atlantic Treaty Organization, Neuilly-sur-Seine Cedex, France*, 1998.

[14] J. Courchesne and A. Laneville. A comparison of correction methods used in the evaluation of drag coefficient measurements for two-dimensional rectangular cylinders. *Journal of Fluids Engineering*, 101(1):506–510, 1979.

[15] R.E. Walpole, R.H. Meyers, S.L. Meyers, and K. Ye. *Probability & Statistics for engineers and scientists.* Pearson Education, Inc., 9th edition, 2012.

Appendix A

Anatomical Definitions of Movements

Flexion: Decreasing the angle of the joint (bending).

Extension: Increasing the angle of the joint (Straightening).

Abduction: Moving a limb away from the centre line of the body.

Adduction: Moving a limb towards the centre line of the body.

(a) **(b)** **(c)**

Figure A.1: Flexion and extension of the hip and the knee showed in (a), flexion and extension of the elbow showed in (b) and abduction and adduction of the arms in (c).

Appendix B

Frontal Area Measurements

B.1 Black/white converter

```
clc
clear all
close all

RGB = imread('picture.png'); %Picture input
Igray= rgb2gray(RGB);
threshold= 30; %Chosen threshold for each pixels
Ibw= Igray> threshold;
imshow(Ibw)
```

B.2 Black pixels counter

```
clc
clear all
close all
%
Image = imread('picture.png'); %Picture input
%
xmax=761; ymax=462; %Picture size
%
White_pix=0; Black_pix=0;
%
for j=1:(xmax)-1
    for i=1:(ymax)-1
        if Image(i,j)==0
            Black_pix=Black_pix+1;
        else
            White_pix=White_pix+1;
        end
    end
end
%
B=Black_pix; %Numbers of black pixels
C=42187.7; %Calibration factor pix/m^2
%
Areal=B/C
```

Appendix C

Raw Data from Experiments

C.1 Experiment 1

Arm angle

When the arms are placed in front of the body of the test subject the arm angle is defined as -10° for all measurements of the arm angle.

Table C.1: The result from the arm angle tested in the wind tunnel. The results are from a low hockey position with knee angle 80°, hip angle 40° and elbow angle 180°.

Arm angle [°]	C_D[ ]	Change [%]	A [m^2]	Change [%]	C_DA [m^2]	Change [%]
90	0.722	0	0.392	0	0.283	0
40	0.712	-1.4	0.401	2.1	0.279	-1.4
30	0.735	1.8	0.394	0.3	0.289	1.8
20	0.743	2.9	0.396	0.9	0.292	2.9
10	0.794	9.9	0.385	-1.9	0.311	9.9
0	0.852	18.0	0.368	-6.3	0.334	18.0
-10	0.637	-11.8	0.299	-23.8	0.190	-32.9

Elbow angle

Table C.2: The results from the elbow angle tested in the wind tunnel. The results are from an upright position with knee angle 150°, hip angle 160° and arm angle 0°.

Elbow angle [°]	C_D[ ]	Change [%]	A [m^2]	Change [%]	C_DA [m^2]	Change [%]
180	0.826	0	0.615	0	0.508	0
160	0.807	-2.3	0.603	-1.9	0.486	-4.2
130	0.776	-6.0	0.589	-4.2	0.457	-9.9
120	0.773	-6.4	0.583	-5.1	0.451	-11.1
110	0.760	-8.1	0.584	-4.9	0.444	-12.6
100	0.765	-7.4	0.577	-6.1	0.441	-13.1
90	0.758	-8.2	0.575	-6.5	0.436	-14.1

C.2 Experiment 2

Hip-knee motion

Table C.3: The results from the hip and knee angles tested in the wind tunnel. The arm angle is 90° and the elbow angle is 180°. The change is the percentage change from the reference position.

Knee [°]	Hip [°]	C_D [ ]	Change [%]	A [m^2]	Change [%]	C_DA [m^2]	Change [%]
150	160	0.715	100	0.576	100	0.412	100
150	90	0.699	97.8	0.421	73.0	0.294	71.4
130	120	0.660	92.4	0.494	85.7	0.326	79.2
120	110	0.641	89.7	0.448	77.8	0.287	69.8
120	70	0.646	90.4	0.380	65.9	0.245	59.5
110	90	0.579	81.1	0.440	76.5	0.255	62.0
110	70	0.613	85.8	0.378	65.6	0.232	56.2
100	60	0.599	83.8	0.348	60.4	0.208	50.6
90	80	0.559	78.2	0.411	71.4	0.230	55.8
90	40	0.603	84.3	0.335	58.2	0.202	49.0
80	50	0.550	76.9	0.361	62.6	0.198	48.1
80	40	0.595	83.3	0.336	58.4	0.200	48.6

Arm angle

When the arms are placed in front of the body of the test subject the arm angle is defined as -10° for all measurements of the arm angle.

Table C.4: The first results ($TS2'$) from the arm angle tested in the wind tunnel. The results are from an upright position with knee angle 150°, hip angle 160° and elbow angle 180°.

Arm angle [°]	C_D [ ]	Change [%]	A [m^2]	Change [%]	C_DA [m^2]	Change [%]
90	0.731	0	0.566	0	0.414	0
80	0.729	-0.3	0.565	-0.2	0.413	-0.3
60	0.722	-1.3	0.514	-9.1	0.408	-1.3
30	0.743	1.7	0.540	-4.6	0.421	-1.7
20	0.780	6.8	0.523	-7.7	0.442	6.8
10	0.821	12.3	0.542	-4.3	0.465	12.3
0	0.835	14.3	0.532	-5.9	0.473	14.3
-10	0.702	-3.9	0.461	-18.4	0.324	-21.7

Table C.5: The second results ($TS2^*$) from the arm angle tested in the wind tunnel. The results are from a position with knee angle 110°, hip angle 90° and elbow angle 180°.

Arm angle [°]	C_D [ ]	Change [%]	A [m^2]	Change [%]	C_DA [m^2]	Change [%]
90	0.601	0	0.400	0	0.250	0
70	0.595	-1.1	0.402	0.6	0.247	-1.1
60	0.588	-2.2	0.411	3.0	0.244	-2.2
40	0.573	-4.6	0.419	4.8	0.238	-4.6
30	0.580	-3.5	0.421	5.3	0.241	-3.5
0	0.718	19.4	0.361	-9.7	0.298	19.4
-10	0.513	-14.7	0.341	-15.1	0.175	-29.9

Elbow angle

Table C.6: The first results from the elbow angle tested in the wind tunnel. The results are from an upright position with knee angle 150°, hip angle 160° and arm angle 90°.

Elbow angle [°]	C_D [ ]	Change [%]	A [m^2]	Change [%]	C_DA [m^2]	Change [%]
180	0.697	0	0.569	0	0.397	0
150	0.685	-1.7	0.548	-3.8	0.375	-5.4
140	0.692	-0.7	0.532	-6.6	0.368	-7.2
130	0.690	-1.0	0.525	-7.8	0.363	-8.6
120	0.690	-1.1	0.514	-9.7	0.356	-10.3
110	0.684	-1.8	0.515	-10.2	0.352	-11.3

Table C.7: The second results from the elbow angle tested in the wind tunnel. The results are from a position with knee angle 90°, hip angle 40° and arm angle 0°.

Elbow angle [°]	C_D [ ]	Change [%]	A [m^2]	Change [%]	C_DA [m^2]	Change [%]
180	0.592	0	0.342	0	0.202	0
120	0.597	0.8	0.300	-12.3	0.790	-11.6
70	0.565	-4.7	0.300	-12.1	0.168	-17.0
60	0.565	-4.7	0.290	-15.0	0.164	-19.0

Turning motion

Table C.8: Position 1 from the turning motion. Arm angle was 90° and elbow angle was 180°.

Left knee [°]	Right knee [°]	Left hip [°]	Right hip [°]	A [m^2]	C_D [ ]	C_DA [m^2]
150	150	170	170	0.559	0.708	0.396
75	150	130	170	0.555	0.715	0.397
60	150	125	170	0.551	0.713	0.393
40	150	70	170	0.545	0.713	0.388

Table C.9: Position 2 from the turning motion. Arm angle was 90° and elbow angle was 180°.

Left knee [°]	Right knee [°]	Left hip [°]	Right hip [°]	A [m^2]	C_D [ ]	C_DA [m^2]
110	110	80	80	0.404	0.582	0.235
75	110	45	80	0.386	0.584	0.226
60	110	35	80	0.372	0.571	0.213
40	110	30	80	0.370	0.574	0.212

Validation positions

Table C.10: Percentage difference between the C_DA from the experiment,C_DA_e, and the C_DA from the model, C_DA_m, from the three validation position.

Pos	Knee [°]	Hip [°]	Right arm [°]	Left arm [°]	C_DA_e [m^2]	C_DA_m [m^2]	Diff [%]
1	145	155	80	30	0.407	0.404	0.9
2	120	130	50	70	0.341	0.337	1.1
3	100	90	60	40	0.243	0.243	-0.2

C.3 Experiment 3

Test subject 3

Table C.11: Angles in the three position tested on $TS3$.

Position	Knee angle [°]	Hip angle [°]	Arm angle [°]	Elbow angle [°]
1	150	160	90	180
2	140	90	90	180
3	85	40	90	180

Table C.12: C_D, A, C_DA_e and C_DA_m and the percentage value of the reference position in the three positions tested. C_DA_e is the experimental result and C_DA_m the modeled result.

Position	C_D [ ]	Diff [%]	A [m^2]	Diff [%]	C_DA_e [m^2]	Diff [%]	C_DA_m [m^2]	Diff [%]
1	0.727	100	0.682	100	0.496	100	0.501	100
2	0.715	98.3	0.460	67.4	0.328	66.1	0.332	66.3
3	0.550	75.7	0.436	63.9	0.240	48.4	0.245	48.9

Test subject 4

Table C.13: Angles in the three position tested on $TS4$.

Position	Knee angle [°]	Hip angle [°]	Arm angle [°]	Elbow angle [°]
1	150	160	90	180
2	130	70	90	180
3	80	40	90	180

Table C.14: C_D, A, C_DA_e and C_DA_m and the percentage value of the reference position in the three positions tested. C_DA_e is the experimental result and C_DA_m the modeled result.

Position	C_D [ ]	Diff [%]	A [m^2]	Diff [%]	C_DA_e [m^2]	Diff [%]	C_DA_m [m^2]	Diff [%]
1	0.730	100	0.687	100	0.501	100	0.504	100
2	0.618	84.7	0.491	71.5	0.303	60.5	0.310	61.5
3	0.539	73.8	0.459	66.8	0.247	49.3	0.242	48.0

Test subject 5

Table C.15: Angles in the three position tested on $TS5$.

Position	Knee angle [°]	Hip angle [°]	Arm angle [°]	Elbow angle [°]
1	150	160	90	180
2	140	100	90	180
3	90	70	90	180

Table C.16: C_D, A, C_DA_e and C_DA_m and the percentage value of the reference position in the three positions tested. C_DA_e is the experimental result and C_DA_m the modeled result.

Position	C_D [ ]	Diff [%]	A [m^2]	Diff [%]	C_DA_e [m^2]	Diff [%]	C_DA_m [m^2]	Diff [%]
1	0.725	100	0.649	100	0.470	100	0.476	100
2	0.681	93.9	0.484	74.6	0.330	70.2	0.338	71.0
3	0.534	73.7	0.465	71.6	0.248	52.8	0.251	52.7

Test subject 6

Table C.17: Angles in the three position tested on $TS6$.

Position	Knee angle [°]	Hip angle [°]	Arm angle [°]	Elbow angle [°]
1	150	160	90	180
2	120	80	90	180
3	90	70	90	180

Table C.18: C_D, A, C_DA_e and C_DA_m and the percentage value of the reference position in the three positions tested. C_DA_e is the experimental result and C_DA_m the modeled result.

Position	C_D [ ]	Diff [%]	A [m^2]	Diff [%]	C_DA_e [m^2]	Diff [%]	C_DA_m [m^2]	Diff [%]
1	0.729	100	0.695	100	0.507	100	0.510	100
2	0.604	82.9	0.519	74.7	0.313	61.7	0.307	60.2
3	0.565	77.5	0.488	70.2	0.276	54.4	0.269	52.7

Field results

Table C.19: Mean values from field experiments in the three different positions tested on $TS6$.

Position	Time [s]	Velocity [m/s]	Drag force [N]	C_DA [m^2]
1	0.63	32.5	-130.3	0.227
2	0.63	33.0	-175.7	0.297
3	0.63	32.2	-166.4	0.295

Appendix D

Anthropometric Measurements of Test Subjects

Different measurements made on the test subjects.

1. Weight [kg]
2. Length (head to feet) [cm]
3. Back shoulder width [cm]
4. Length (crotch to floor) [cm]
5. Arm length (shoulder to wrist) [cm]
6. Chest circumference [cm]
7. Hip circumference [cm]
8. Arm circumference [cm]
9. Thigh circumference [cm]

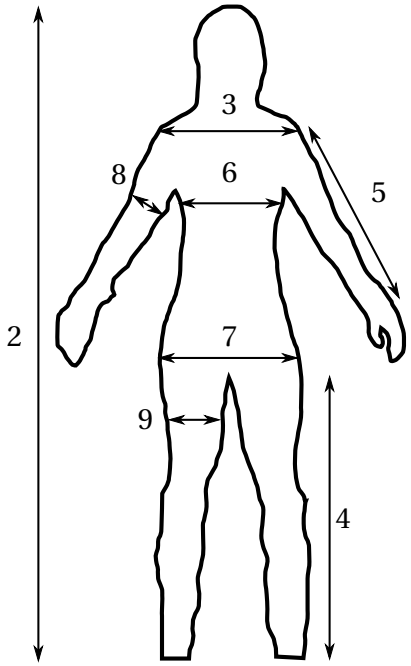

Table D.1: Body measurements of test subjects

	1	2	3	4	5	6	7	8	9
$TS2$	72	171	45	77	53	99	92	35	59
$TS3$	91	180	49	86	68	104	103	33	65
$TS4$	95	183	52	89	57	107	109	34	65
$TS5$	83	187	55	93	64	102	96	30	58
$TS6$	100	185	56	86	60	108	109	35	67

Appendix E

Numerical Model

```
function [totCd] = CdFunc(A,B,Cr,Dr,Cl,Dl)
%Hip/knee motion-----------------------------------------------------
%Defining the range of movement:
%Empty matrix 160*160:
jmax=160;
CdA = zeros(jmax);
%
%The method for the upper part of the range of movement
CdA(jmax,jmax)=100; %Reference position
dx=-0.45; %Change in CdA in x-direction for hip angle > 90 degrees
dy=-0.25; %Change in CdA in y-direction for hip angle > 90 degrees
%
for j=1:jmax
        j1=jmax-(j-1);
    for i=1:jmax
        i1=jmax-(i-1);
        CdA(j1,i1)= CdA(jmax,jmax)+(i-1)*dx+(j-1)*dy;
    end
end
%
```

```
%The method for the lower part of the range of movement
CdA(80,40)=48.6; %Hockey position (lowest position) relative ref.postition
dx=0.09; %Change in CdA in x-direction for hip angle < 90 degrees
dy=0.22; %Change in CdA in y-direction for hip angle < 90 degrees
%
for j=1:90
      j1=(j-1)+80;
    for i=1:50
        i1=(i-1)+40;
        CdA(j1,i1)= CdA(80,40)+((i-1)*dx+(j-1)*dy);
    end
end
%
% Elbow angle ------------------------------------------------------------
imax=120;
CdAE = zeros(1,imax+1);
dx1=-0.18; dx2=-0.128; %Changes in the different regions
for i=1:59
   CdAE(1,i+1)=(i+1)*dx1;
end
i1=1;
for i=60:89
   CdAE(1,i+1)=i1*dx2+CdAE(1,60);
   i1=i1+1;
end
%
CdAE=CdAE/2;%Assuming that both elbows has the same impact on the CdA
Dr=181-Dr;%Adjusting so the right angle can be an input (right elbow)
Dl=181-Dl;%Adjusting so the right angle can be an input (left elbow)
%
```

```
%ARM angle ------------------------------------------------------------------
imax=100;
CdAA = (-28)*ones(1,imax+1);
dx1=4.5; dx2=-0.65; dx3=0.029;
i1=1;
for i=1:10
    CdAA(1,i+1)=i1*dx1+CdAA(1,1);
    i1=i1+1;
end
i2=1;
for i=11:39
    CdAA(1,i+1)=i2*dx2+CdAA(1,11);
    i2=i2+1;
end
i3=1;
for i=40:100
    CdAA(1,i+1)=i3*dx3+CdAA(1,40);
    i3=i3+1;
end
CdAA=CdAA/2;%Assuming that both elbows has the same impact on the CdA
Cr=Cr+11;%Adjusting so the right angle can be an input (right arm)
Cl=Cl+11;%Adjusting so the right angle can be an input (left arm)
%----------------------------------------------------------------------------
%Cd(Knee,hip,right arm, right elbow, left arm, left elbow)
%
FA = 0.576; %Frontal Area of test subject
RefPos = 0.725*FA; % value in the reference position
totCd = CdA(A,B)+CdAA(1,Cr)+CdAE(1,Dr)+CdAA(1,Cl)+CdAE(1,Dl);%Summing up
totCd = (RefPos*totCd)/100;
end
```